

A SMALL SHIFT MOSSBAUER
SPECTROMETER

by

JOHN LESLIE BEVERIDGE

B.Sc. (Hons.) University of British Columbia, 1965

A THESIS SUBMITTED IN PARTIAL FULFILMENT OF
THE REQUIREMENTS FOR THE DEGREE OF
MASTER OF SCIENCE
IN THE DEPARTMENT OF
PHYSICS

We accept this thesis as conforming to the
required standard

THE UNIVERSITY OF BRITISH COLUMBIA

March, 1968

In presenting this thesis in partial fulfilment of the requirements for an advanced degree at the University of British Columbia, I agree that the Library shall make it freely available for reference and study. I further agree that permission for extensive copying of this thesis for scholarly purposes may be granted by the Head of my Department or by his representatives. It is understood that copying or publication of this thesis for financial gain shall not be allowed without my written permission.

Department of Physics
The University of British Columbia
Vancouver 8, Canada

Date April 11 1968

ABSTRACT

In this thesis a small shift Mossbauer spectrometer developed by the author is described.

An automatic multiplexing and printout system for eight scalars is described along with a digital electronic control system for the motor drive.

Three different suspension systems for the transport portion of the linear drive --

- (1) An air bearing suspension as developed by Wells
- (2) An oil supported teflon bearing suspension
- (3) A leadscrew suspension

have been constructed. Mossbauer spectra for two sources -- Co^{57} in Armco iron and Co^{57} in Pt^{195} -- against an enriched iron absorber have been taken with the latter two suspensions and have been compared with each other and with spectra taken on a commercial Mossbauer spectrometer.

Theoretical calculations of the central Mossbauer line for the Armco iron source and enriched iron absorber have been made using the computer program written by Woodrow. These calculations are compared with the experimental spectra.

TABLE OF CONTENTS

| | | |
|-------------|--|----|
| Chapter I | INTRODUCTION | 1 |
| Chapter II | GENERAL OUTLINE OF THE SMALL SHIFT SPECTROMETER | 6 |
| | 2:1 Requirements and Methods | 6 |
| | 2:2 Electronics and Control System ... | 7 |
| Chapter III | ELECTRONICS | 9 |
| | 3:1 Scalers and Printout System | 9 |
| | 3:2 Gamma Ray Detection System | 13 |
| | 3:3 Setup of Single Channel Analysers | 14 |
| | 3:4 Elapsed Time Measurement | 15 |
| | 3:5 Control System | 15 |
| | 3:6 Scaler Clearing | 17 |
| Chapter IV | VELOCITY MONITORING SYSTEM | 18 |
| Chapter V | TRANSPORT SYSTEMS | 21 |
| | 5:1 Air Track Suspension | 21 |
| | 5:2 Mechanical Drive System I | 26 |
| | 5:3 Leadscrew Suspension | 29 |
| | 5:4 Mechanical Drive System II | 29 |
| Chapter VI | EXPERIMENTAL RESULTS | 33 |
| | 6:1 Oil Supported Teflon Bearing Suspension | 33 |
| | 6:2 Leadscrew Suspension | 39 |
| | 6:3 Comparison | 40 |
| Chapter VII | CONCLUSIONS | 44 |

TABLE OF CONTENTS (cont.)

| | | |
|--------------|-------------------------|----|
| Appendix A | D.E.C. SYMBOLISM | |
| Appendix B | COMPUTER PROGRAMS | |
| Appendix C | | 49 |
| BIBLIOGRAPHY | | 47 |

LIST OF FIGURES

- Figure 1. Electronics and Control System
- Figure 2. Printed Circuit Board for C μ L Scalers
- Figure 3. Block Diagram of Printout and Multiplexing System
- Figure 4. Decade Multiplexing Gates
- Figure 5. Main Shift Register
- Figure 6. Decade Strobe Register and Scale of Eight Counter
- Figure 7. Ring Counter
- Figure 8. Main Pulse Chain
- Figure 9. C μ L 958 -- D.E.C. Buffer
- Figure 10. Detection Electronics
- Figure 11. Co⁵⁷ Pulse Height Spectrum
- Figure 12. Cosmic-C μ L Gated Converter
- Figure 13. Gated Clock Converter
- Figure 14. Control System Electronics
- Figure 15. Control Relay Wiring
- Figure 16. Scaler Clearing Circuit
- Figure 17. Gated Fringe Detector
- Figure 18. Velocity Output for Oil Supported Suspension
- Figure 19. Mechanical Drive System I
- Figure 20. Mechanical Drive System II
- Figure 21. Leadscrew Suspension
- Figure 22. Velocity Output for Leadscrew Suspension
- Figure 23. Mossbauer Spectrum for Armco Iron Source "Eyeball Fit" Curve Oil Supported Suspension

- Figure 24. Mossbauer Spectrum for Armco Iron Source Single Lorentzian Fit Curve, Oil Supported Suspension.
- Figure 25. Mossbauer Spectrum for Armco Iron Source Taken on Commercial Constant Acceleration Spectrometer
- Figure 26. Mossbauer Spectrum for Pt^{195} Source Oil Supported Suspension
- Figure 27. Mossbauer Spectrum for Armco Iron Source "Eyeball Fit" Curve Leadscrew Suspension
- Figure 28. Mossbauer Spectrum for Armco Iron Source Single Lorentzian Fit Curve Leadscrew Suspension
- Figure 29. Mossbauer Spectrum for Pt^{195} source Leadscrew Suspension
- Figure 30. Mossbauer Spectra for Armco Iron Source Oil Supported Suspension and Leadscrew Suspension Superimposed
- Figure 31. Theoretical Curves
- Figure 32. Comparison of Experimental and Theoretical Curves

ACKNOWLEDGEMENTS

I wish to express my gratitude to Dr. B. L. White for his supervision through the course of this work and to Dr. J. B. Warren for his supervision in Dr. White's absence.

I am also grateful for the help of the students and technical staff of the Positron and Van de Graaff groups. Special thanks is due to Mr. R. P. Haines for his patience in the construction of numerous mechanical parts required.

I am indebted to the National Research Council for the two scholarships held during the course of this work and for their continued financial support.

CHAPTER I

INTRODUCTION

There are many mechanisms which may cause the position of the Mossbauer resonance peak to shift from its expected position. These include:

- (1) Internal and external magnetic fields at the site of the absorbing or emitting nucleus.
- (2) A temperature difference between the source and absorber.
- (3) A difference in Debye temperature in the source and absorber.
- (4) A difference in average mass in the source and absorber.
- (5) A difference in chemical environment at the site of the radiating and absorbing nucleus. This is called the "chemical" or "Isomer" shift.
- (6) Localized modes of vibration in the crystal lattice of the source or absorber.

The above effects have been reviewed theoretically by Woodrow⁽²⁾ and some are contained in the references 16, 24, 25.

This list is of course not complete but is representative of the many effects observable by the measurement of shift of the Mossbauer line. Such measurements are usually aimed at the determination of some properties of the host material at the site of the Mossbauer nucleus.

In his thesis of November 1965 Wells⁽¹⁾ proposes a zero phonon Mossbauer experiment to measure the lifetime of localized vibrational modes in a crystal lattice which required the measurement of the shift of the Mossbauer peak. In this thesis Wells reviews some calculations of the ratio of the localized mode frequency to the Debye frequency (ω_{LM}/ω_0) and the lifetime of localized modes (τ_{LM}) for four frequency distributions as a function of the mass defect ϵ where

$$\epsilon = \frac{M_{HOST} - M_{IMPURITY}}{M_{HOST}}$$

The four models used to obtain the frequency distribution were:

(1) Linear Chain: Montroll & Potts, 1955

(2) Debye: Dauber & Elliot, 1963

Maradudin, 1963

(3) Nearest Neighbour simple cubic lattice in which the central and noncentral force constants are equal: Montroll & Potts, 1955

(4) Nearest Neighbour central force face centred cubic: Overton & Dent, 1960

The source and absorber used in such an experiment must be chosen very carefully as shifts due to other effects such as those listed above must be avoided. The source and absorber chosen by Wells were:

Source: 0.0005 inch Pt¹⁹⁵ with 5 mc. Co⁵⁷ as a dilute impurity i.e. 1 part Co⁵⁷ to 1000 parts Pt¹⁹⁵

Absorber: 0.0005 inch Pt¹⁹⁵ with 0.01 mg/cm² Fe⁵⁷

With this source and absorber combination Wells calculates, using the fourth model above, that $\Gamma_{LM} = 3.0 \times 10^{-5} (1 + 0.00964T)$. and $\omega_{LM}/\omega_0 = 1.38$. With these numbers the expected shift of the Mossbauer line due to the localized modes, using an Einstein oscillator approximation, at $T = 300^\circ\text{K}$ is calculated to be $\Gamma_0/300$ where Γ_0 is the natural linewidth of the Co⁵⁷ transition

$$\text{i.e. } \Gamma_0 = 4.5 \times 10^{-9} \text{ ev}$$

Wells calculated that for this source and absorber the count rate for a detector subtending a solid angle of 0.1 steradians would be 35 counts/sec. and that the time required to determine the lineshift to within 10% was 16 weeks. This calculation was made with the assumption that the velocities were exactly constant. i.e. the velocity distribution used was a delta function. This of course is never the case so the above sets only a minimum time limit.

To perform the proposed experiment it was obvious that a very smooth vibration free linear drive system was required. Wells tried to construct such a drive using an air bearing track and rider transport suspension system with a synchronous motor driven tape and pulley drive. It was found however that vibrations in the system, either mechanically or aerodynamically induced made the drive constructed completely useless for the above application.

The construction of a drive system which produces sufficiently stable velocities to do the proposed experiment is extremely difficult. There have been many means tried for producing the velocities necessary for observing the Mossbauer Effect. A few of these can be seen in references 3, 4, 5, 6, 7, 18. For the measurement of small shifts of the central line position the most convenient type is that which produces a constant velocity. The most successful scheme for doing this conveniently seems to be the use of a leadscrew and carriage, provided that no large weights are to be transported. Such transports have quite a large amount of friction inherent in them, even when well machined and aligned, and therefore have some vibrational noise associated with them. The air bearing described by Wells should, at least in principle, greatly decrease the friction in the transport system and thus decrease the vibrational noise present in the system. There are however practical problems in the stability of such a suspension.

This thesis presents the development of a small shift Mossbauer spectrometer which it is hoped will be sufficiently precise to perform the proposed experiment. The counting and control electronics developed are described. The laser interferometer and fringe detection system used as a velocity measurement system are described. A comparison has been made of three suspension systems, the air bearing suspension developed by Wells, an oil suspension with teflon guides and a leadscrew system constructed by the author.

CHAPTER II

GENERAL OUTLINE OF THE SMALL SHIFT

MOSSBAUER SPECTROMETER

2:1. Requirements and Methods

To determine the position of the Mossbauer peak it is sufficient to measure the count rate at four discrete velocities. If we are concerned with a resonance approximately centered at zero velocity we may choose these velocities to be $\pm V_1$ and $\pm V_2$. The shift of the line position can then be given by the following formula

$$\Delta V = \left(\frac{\delta V}{2} \right) \left[\frac{(N_{V_1} + N_{V_2}) - (N_{-V_1} + N_{-V_2})}{(N_{-V_1} + N_{V_1}) - (N_{-V_2} + N_{V_2})} \right]$$

where:

N_{V_i} = number of counts at the velocity V_i

$\delta V = V_1 - V_2$

ΔV = shift of the line position from $V=0$

This formula assumes that $\pm V_1$ and $\pm V_2$ are contained in a linear range of the resonant spectrum and that the shift ΔV is small.

There are basically two methods of measuring shifts of the above form. The first and experimentally the least complex is to store the counts for each velocity in separate scalers and from the total collected over the entire experiment calculate the

count rate at each velocity and hence the position of the peak. This method is not applicable to the present experiment as 16 weeks of counting time are expected to be required and electronics which are stable over this period of time would be difficult if not impossible to obtain.

The alternative method, and the one used here, is to printout or store in some manner the number of counts after a single traversal and to run the four velocities in successive traversals. This enables the calculation of the line position after four traversals which will involve times of the order of hours. Electronics which are stable for this amount of time are readily available. Statistics can then be taken on a number of calculated line positions instead of on the number of counts at one particular velocity.

2.2. Electronics and Control System

The general outline of the electronics and control system for the small shift Mossbauer spectrometer used in this work is shown in Fig. (1). The eight scalers record the following:

- (1) number of counts in the resonance channel
- (2) number of counts in the background channel
- (3) elapsed time
- (4) distance travelled

The program generator controls the printout of the

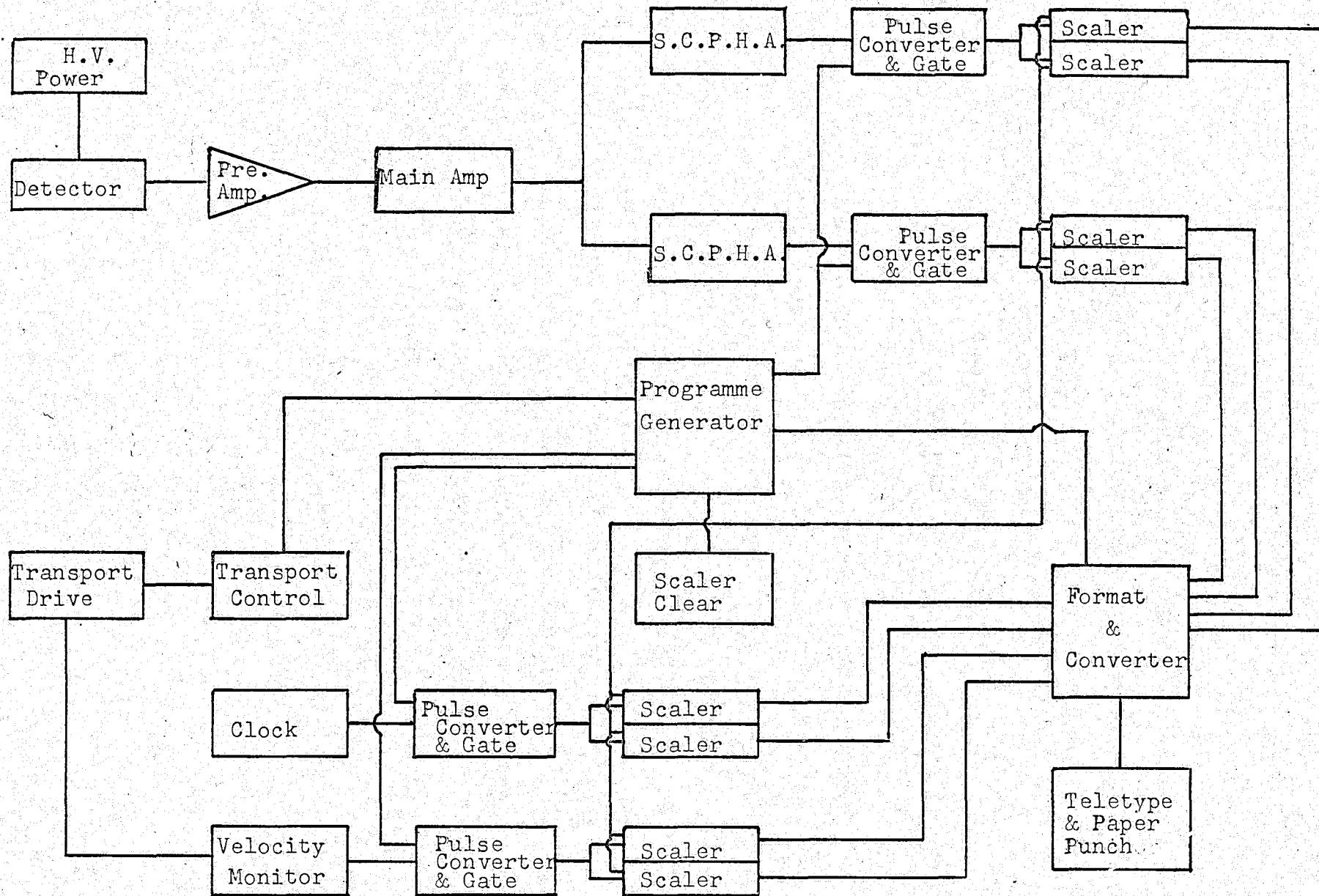


Figure 1. Block Diagram of Electronics and Control System

scalars and the direction and velocity of the linear drive system. In the present application the program generator produces the following sequence of events at the end of each traversal of the transport system:

- (1) The scalars are gated off.
- (2) The motor is shut off after a 3 second delay.
- (3) The motor is reversed.
- (4) The scalars are printed out and cleared.
- (5) Power is restored to the motor.
- (6) The velocity is changed between two discrete values. This happens only on every second traversal.
- (7) The scaler gates are opened.

The printout of the scalars is done on an A.S.R.-33 teletype which is equipped with a paper tape punch. This greatly simplifies the analysis of the data obtained as the tape is readily processed by the P.D.P.-8 computer available in the lab, however it requires the construction of a formatting and code conversion unit. This unit converts the binary coded decimal (B.C.D.) output code of the scalars to the serial teletype code and determines the format in which the scalars are printed out.

CHAPTER III

ELECTRONICS

3:1 Scaling and Printout Systems

Since scalers were not, at the time, commercially available with automatic printout systems, eight 10^7 scalers were constructed from Fairchild micrologic integrated circuit decade counters. Two of these scalers were mounted on a single printed circuit board (Fig. 2) with 36 connector pins which fit in two Digital Equipment Corporation (D.E.C.) connector blocks. These scalers were multiplexed together by means of four 18 pole single throw Coto Coil reed relays placed between the counter output leads and the common output pins.

The binary coded decimal (B.C.D.) to teletype converter and multiplexing system is shown in Figures 3-8. This system was constructed from D.E.C. modules and the symbolism is that used by D.E.C. (App. A). The levels from the decade counters are converted to D.E.C. levels by the buffers (Fig. 9) and put onto the inputs of the R141 multiplexing gates (Fig. 4) which form data bits 5, 6, 7 and 8. These gates perform the function of multiplexing the outputs of the seven decade counters of each scaler. Each R141 module is a seven input AND gate and each section may be examined individually by a -3 volt signal on one input. The output of the gate is then the inverse of the level

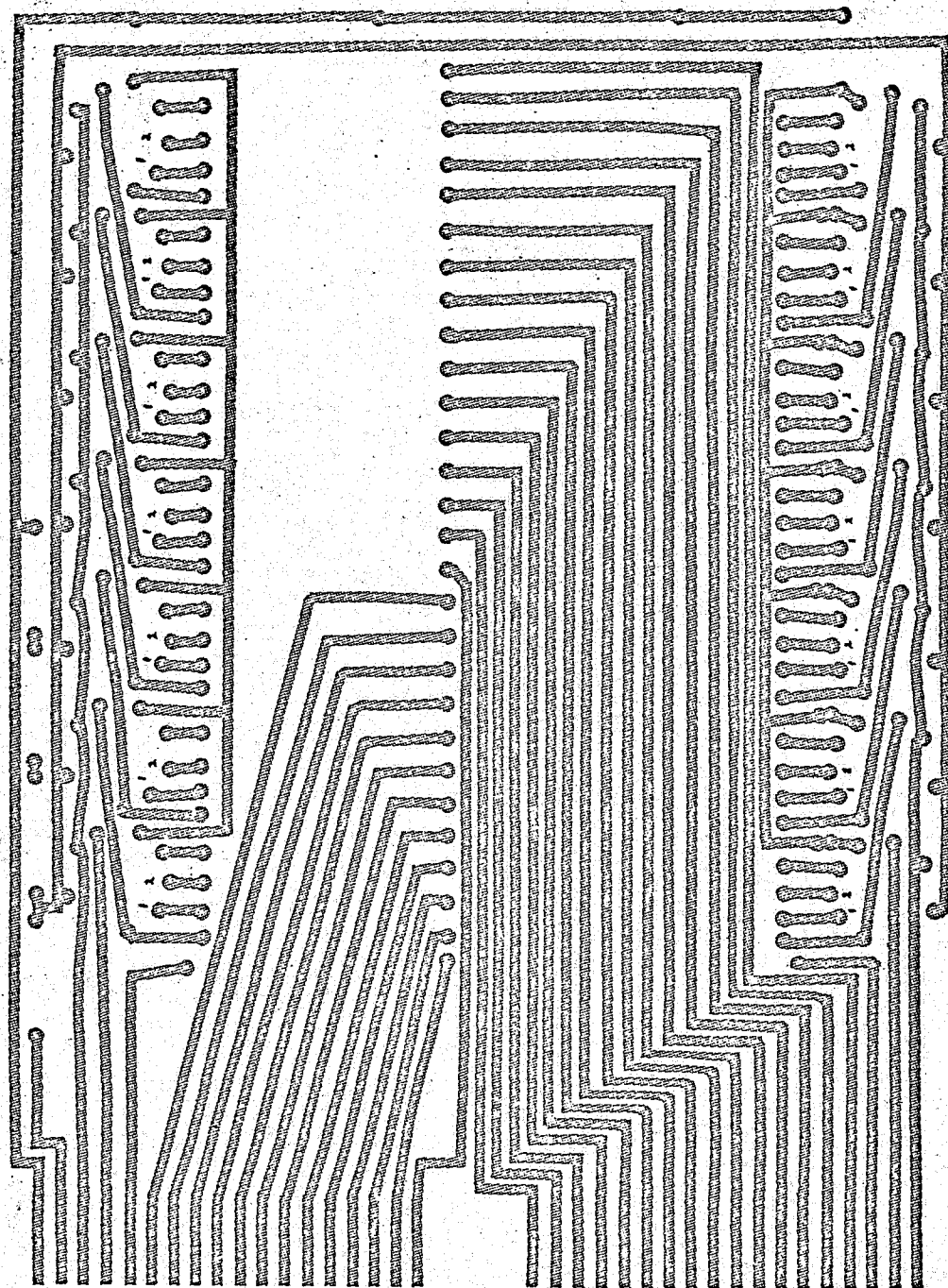


Figure 2. Printed circuit board for C L 958 integrated circuit scalars.

on the other input of that section provided that at least one input of each of the other six sections is at ground. Thus by applying -3 volt levels in sequence to the gate sections i.e. Load A, Load B etc. the outputs of the decade counters can be scanned individually. The other inputs on these data bits are fixed and are used to produce carriage return (C.R.) line feed (L.F.) and space (S.P.) codes. Data bits 3 and 4 are required only for C.R. L.F. and S.P. codes and are fixed for scaler inputs.

Data bits 3 to 8 are used for the level inputs for the diode capacitor diode (D.C.D.) gates of the R205 flip flops in the main shift register (Fig. 5). The other level inputs of the eleven bit register are fixed to produce the teletype code for numbers C.R. L.F. and S.P. Upon the pulse signal, Load T₁₀, the information on these level inputs is loaded into the shift register. The T₁₀ flip flop will always produce a ground output on its "0" terminal which will cause the T₁₀=0 level to go to -3 volts and allow the "Out Active" flip flop to change state when the next clock pulse comes. The change of state of the "Out Active" flip flop enables the pulse amplifier (P.A.) gate and loads a -3 volt level into the "1" output of the "Line" flip flop which is the starting bit of the teletype code. Succeeding clock pulses shift the register at a rate chosen to give the correct timing for the teletype, until the -3 volt level on the "0" output of the "T₁₀" flip flop is loaded into the "count

11" flip flop. At this point all the inputs to the R111 gates are at -3 volts and the level T10=0 is ground. The next clock pulse then shifts the register once more to give the second teletype stop bit and changes the state of the "Out Active" flip flop to terminate the printout procedure until another Load T10 signal is received.

The above action enables the printout of one of the B.C.D. decade counters and is the main part of the code conversion unit. The rest of the electronics is for forming and multiplexing the decade counters and scalars.

The shift register (Fig. 6) is used to strobe the decade counters via the R141 multiplexing gates (Fig. 4) and the ring counter (Fig. 7) is used to strobe the eight scalars. Pulses which control these units come from the main pulse chain (Fig. 8).

When the power is turned on the system is set up to print by the switches indicated. The ring counter must be cleared and a "1" loaded into the "Stop" flip flop. The scale of eight counter (Fig. 6) is set up to give a ground output from the R111 gate when it is advanced one unit and a "1" is loaded into the "Space" flip flop. This insures that C.R. and L.F. are the first characters to be printed.

When a -3 volt level is applied to the Print input, the Schmitt Trigger gives out a pulse which will pass through

the B104 gates, advance the scale of eight counter, clear the decade strobe register and advance the ring counter to pull in the reed relays on the first scaler. One microsecond later the same pulse loads a "1" into the "C.R." flip flop of the decade strobe register which strobes the C.R. section of the R141 multiplexing gates and puts the appropriate levels on the data bits. Two milliseconds after the initial pulse -- this time was chosen to insure that the Coto Coil switches were closed -- the "Load T10" pulse loads these levels into the main shift register and the character is printed out on the teletype as described above.

If the print level is at -3 volts when the "Out Active" flip flop changes state at the end of a printout this change of state gives another pulse from the Schmitt Trigger output. This second pulse will pass through the B104 gates, shift the decade strobe register to put the L.F. code on the data bits and 2 msec. later this character is printed out as above. The "Load Shift Register", "Shift Ring Counter" and "Print Counter" lines are now disabled as there is a "0" in the "Space" flip flop and thus none of these actions is carried out by the second pulse.

The above action proceeds until the first scaler has been printed out and the "Space" flip flop has been loaded with a "1". After the space has been printed the next pulse from the Schmitt Trigger advances the scale of eight counter and advances

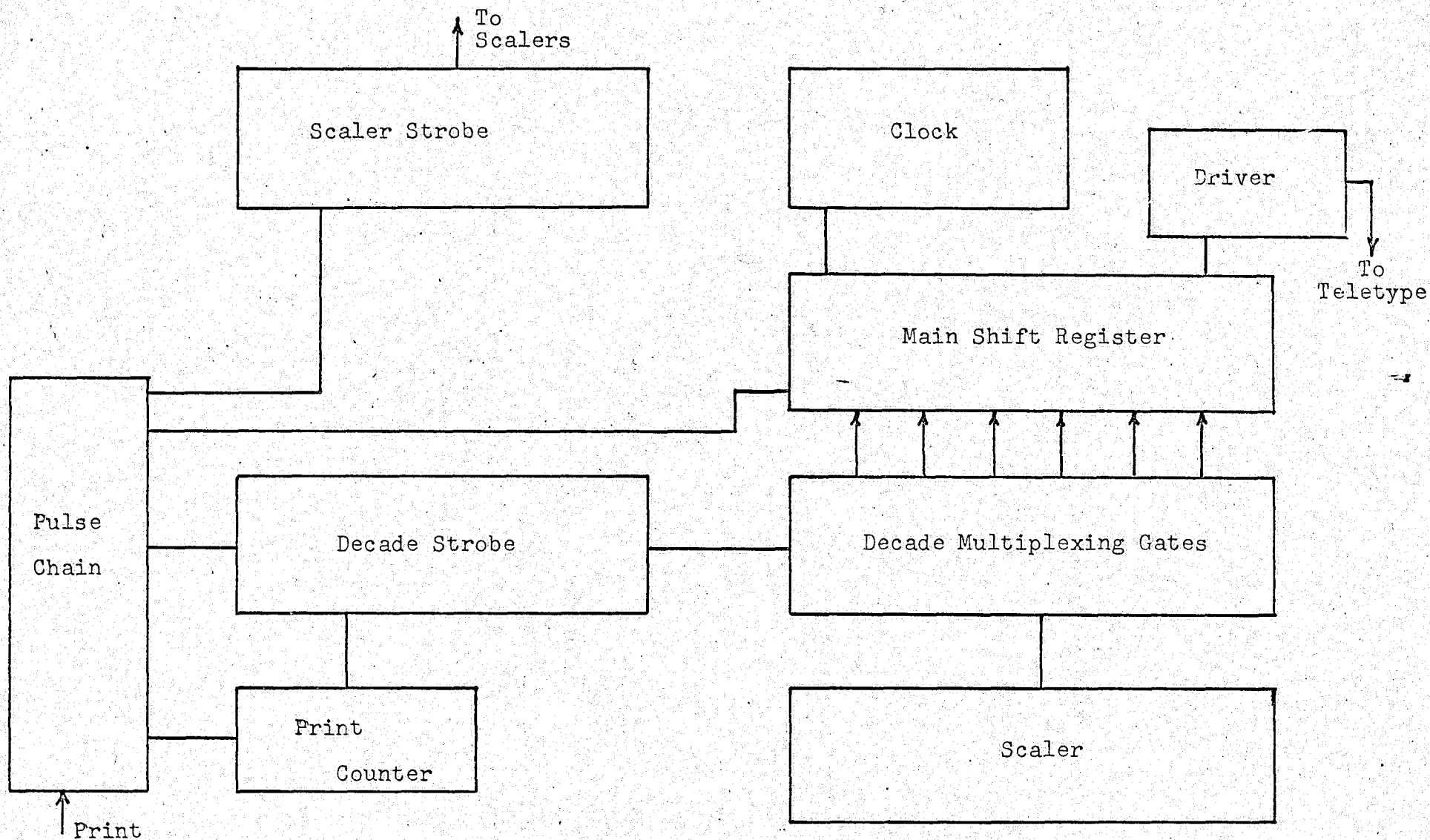


Figure 3. Block Diagram of Printout and Multiplexing System

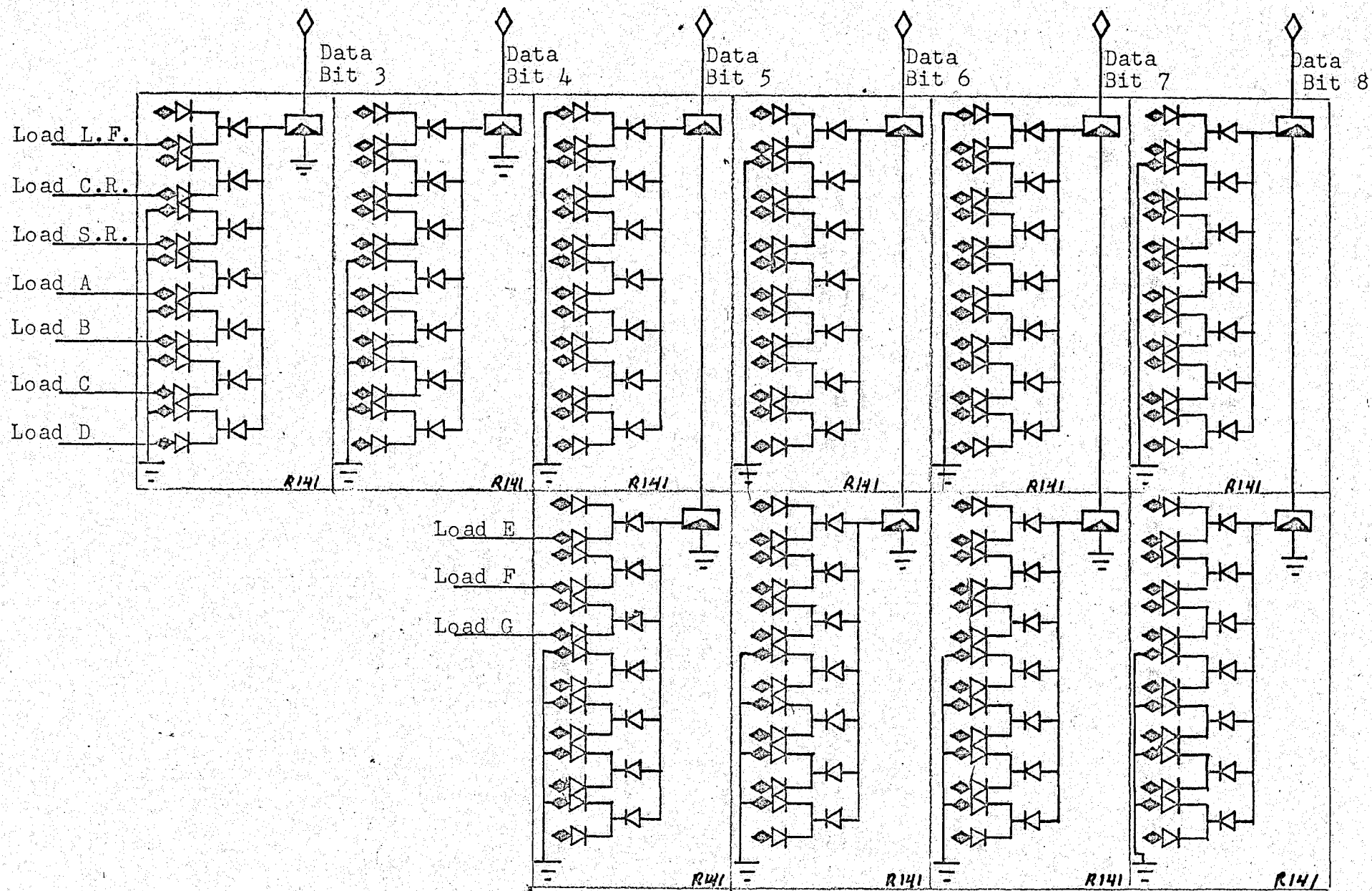


Figure 4. Decode Multiplexing Gates

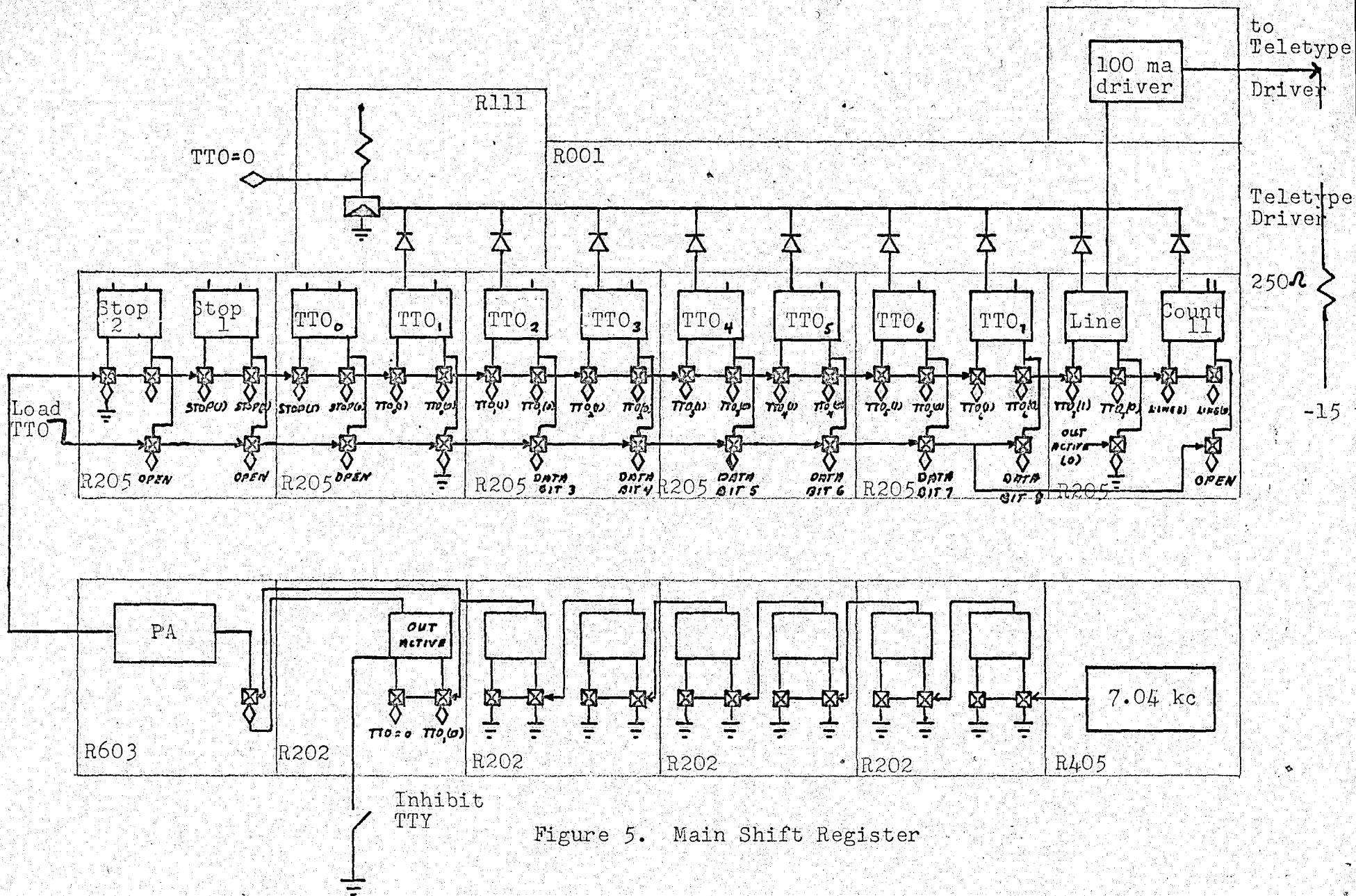


Figure 5. Main Shift Register

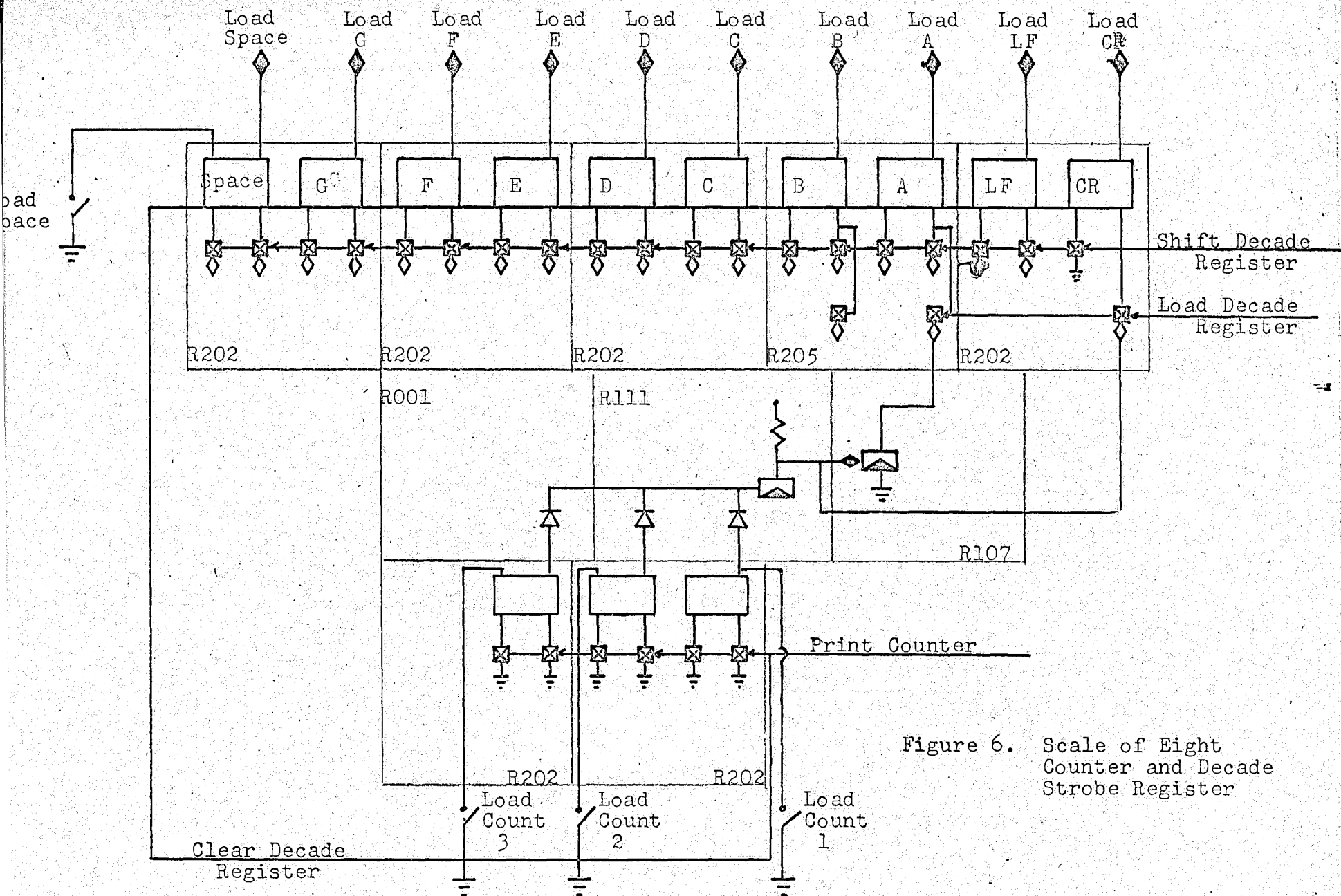


Figure 6. Scale of Eight Counter and Decade Strobe Register

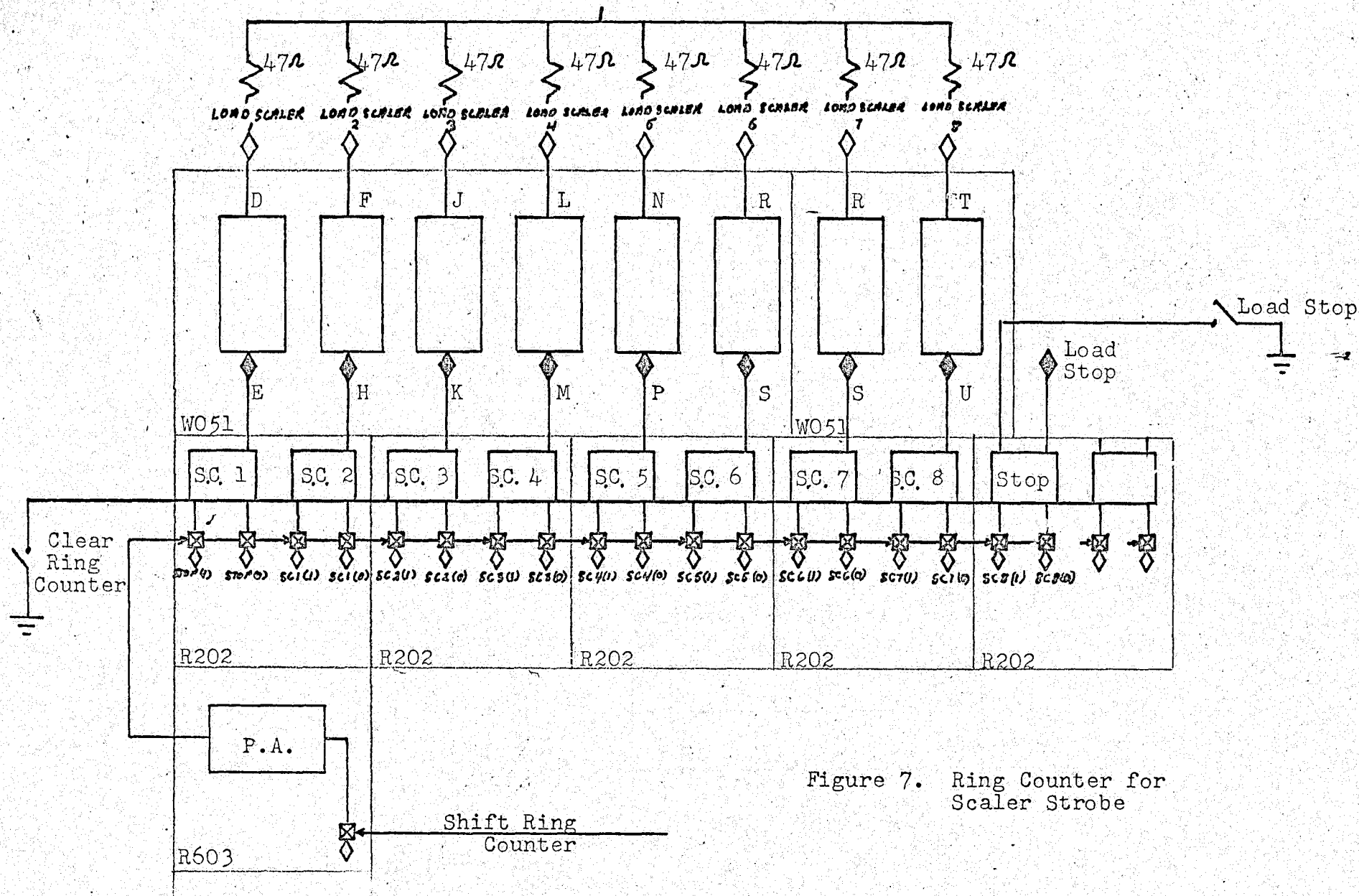


Figure 7. Ring Counter for Scaler Strobe

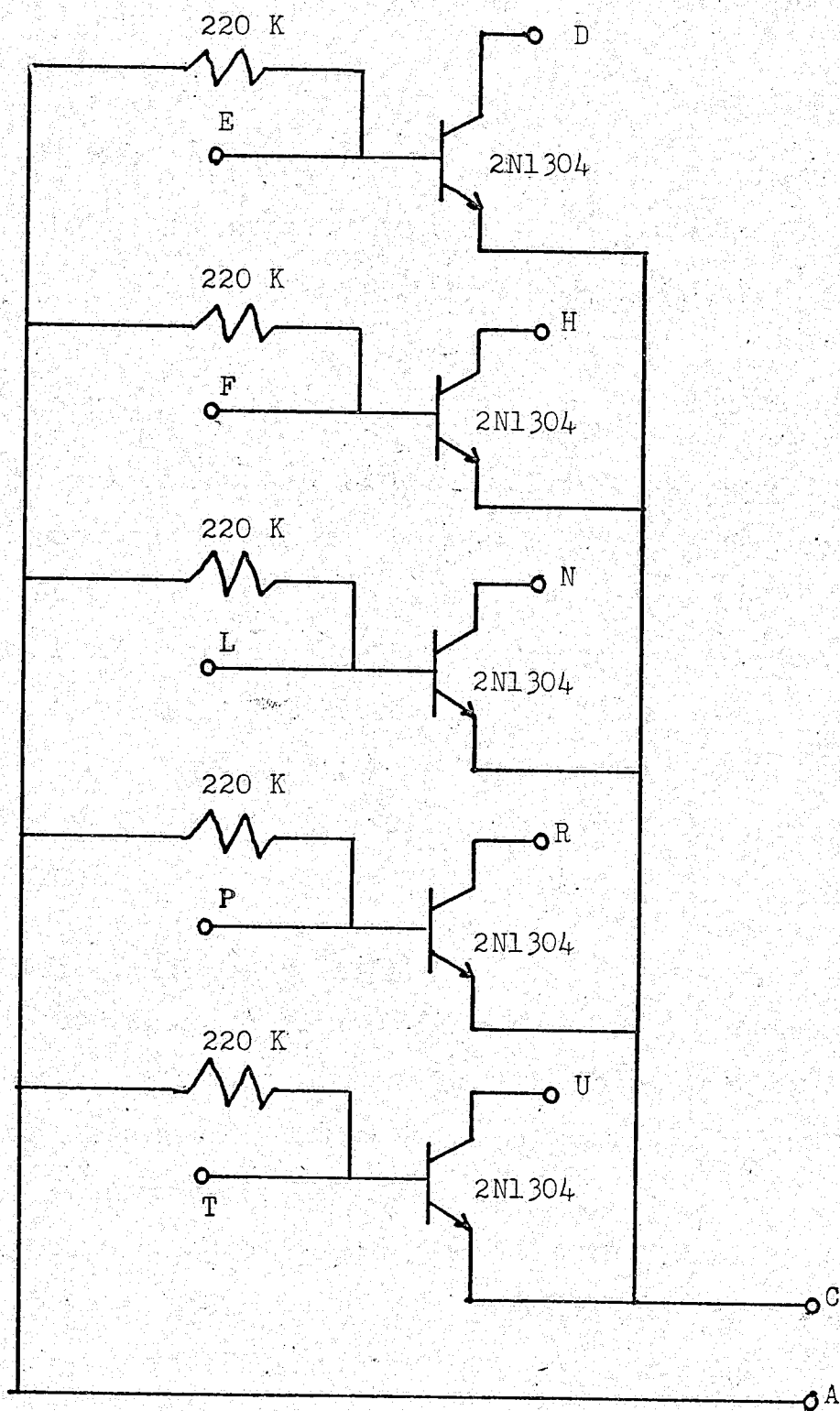


Figure 9. C L 958 - D.E.C. Buffer Circuits.
(This circuit is mounted on a printed circuit board).

the ring counter to scaler two. The output of the R111 gate on the scale of eight counter is now negative so the "Load Decade Register" pulse loads a "1" into the "A" flip flop. The second scaler is then printed out as above without the C.R. and L.F. characters.

The above procedure continues until all eight scalars have been printed out. When the two flip flops "S.C.8" and "Space" both contain "1's", which will happen when a space has been printed after the eighth scaler has been printed, the B104 gates will not transmit the Schmitt Trigger pulse. The pulse obtained after the space has been printed then serves only to shift the ring counter to load a "1" into the "Stop" flip flop. The printout is thus terminated, but is set up to receive another print signal.

3:2 Gamma Ray Detecting System

The electronics used for detecting and counting gamma rays in this experiment is shown in block form in Fig. 10. The units used were standard commercial equipment as listed below.

Dynatron Type 1430 A preamp

Cosmic Model 901 A double delay line amplifier

Reuter Stokes model 30 A proportional counter

Fluke model 412 B high voltage power supply

Cosmic model 901 SCA single channel analysers

A typical pulse height spectrum of the Co^{57} in Fe source

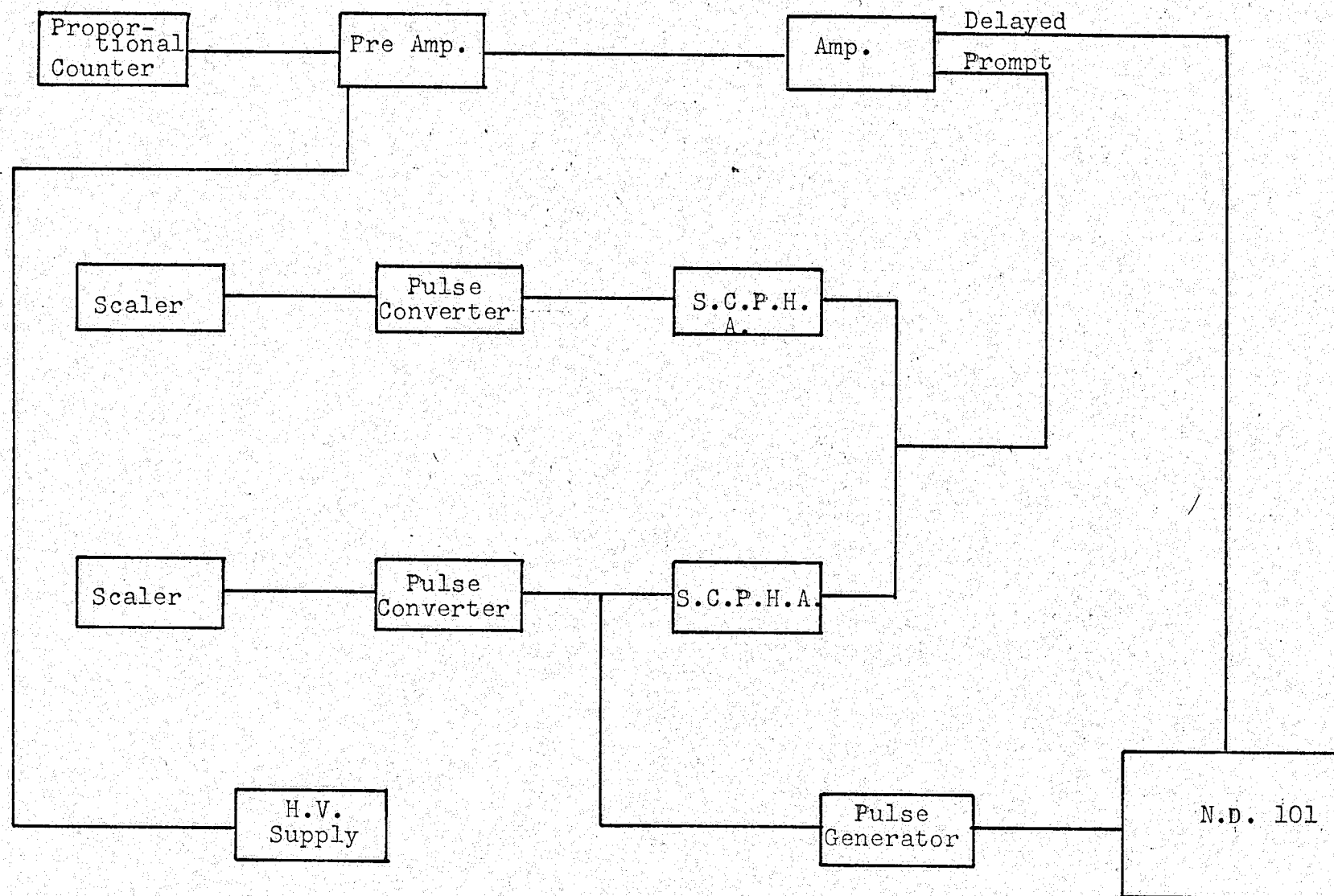


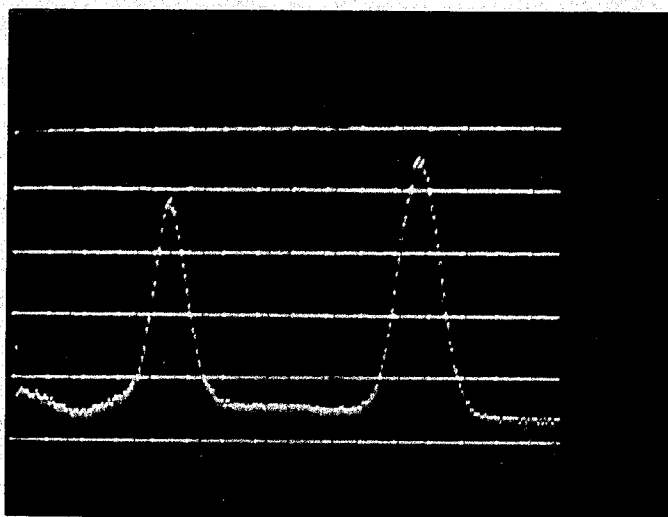
Figure 10. Block Diagram of the Detection Electronics.

used in this experiment is shown in Fig. 11. In this spectrum the intensity of the 6.8 Kev peak was reduced relative to the 14.4 Kev peak by placing an aluminium foil over the beryllium window of the proportional counter. This spectrum shows a resolution of 10.6% F.W.H.M. for the 14.4 Kev line which is better than the 11.3% resolution of the spectrum supplied by the manufacturers with the counter.

3:3 Setup of Single Channel Analysers

The single channel analysers were set up to accept only certain parts of the pulse height spectrum by operating the ND 101 kicksorter used in a coincidence mode. The input to the kicksorter was taken from the delayed output of the Cosmic amplifier and coincidence pulses from a Datapulse pulse generator triggered by the output of the single channel analyser. The internal delay and pulse width of the pulse generator were adjusted so that the coincidence pulses overlapped the analysed pulses when the two were observed on a dual beam scope. In this mode of operation the kicksorter only analysed pulses passed by the single channel analyser. One single channel analyser was set up in this way to accept pulses only in the 14.4 Kev peak and the other to accept pulses between the 6.8 Kev and 14.4 Kev peaks over the same number of channels as included in the 14.4 Kev peak.

The cosmic single channel analysers give output pulses of either polarity of six volt amplitude and 150 nanosecond duration. These are not compatible with the positive 1.5 volt 200



Co⁵⁷ pulse height spectrum

| | |
|-----------------------------|--------------|
| 6.8 Kev peak | channel 72 |
| 14.4 Kev peak | channel 198 |
| FWHM of 14.4 Kev peak | 25 channels |
| FWHM of 6.8 Kev peak | 21 channels |
| Resolution of 14.4 Kev peak | 10.6% |
| Resolution of 6.8 Kev peak | 19.2% |
| High Voltage | 2030.2 volts |
| Cosmic Amplifier Gain | 1.2 |

Figure 11. Pulse Height Spectrum for Co⁵⁷

nanosecond pulses required by the integrated circuit counters. The negative output was therefore gated and converted to the required pulses by the circuit in Fig. 12 which was mounted on a blank D.E.C. circuit board. The 68 pf capacitor on the emitter of the input transistor provides sufficient pulse stretching to give an output pulse of 600 nanosecond duration.

3:4 Elapsed Time Measurement

The 7.04 kilocycle R405 clock used in the code conversion unit was used to measure elapsed time during the course of this experiment. The stability of the clock frequency is quoted to be 0.01 per cent of the quoted value between 0°C and 55°C. This then when gated at the beginning and end of each traversal of the transport system provides an accurate stable determination of the time taken for the traversal.

The clock pulses are of 100 nanosecond duration and rise from -3 volt to ground. These pulses were gated and converted to the 1.5 volt 200 nanosecond positive pulses required by the scalars by the circuit in Fig. 13. This circuit was also mounted on a blank D.E.C. circuit board.

3:5 Control System

The electronics of the control system is shown in Fig. 14. This system, like the code conversion system, was built from D.E.C. modules and the symbolism is that of D.E.C.

The LS 230 photo cells are mounted beside the transport

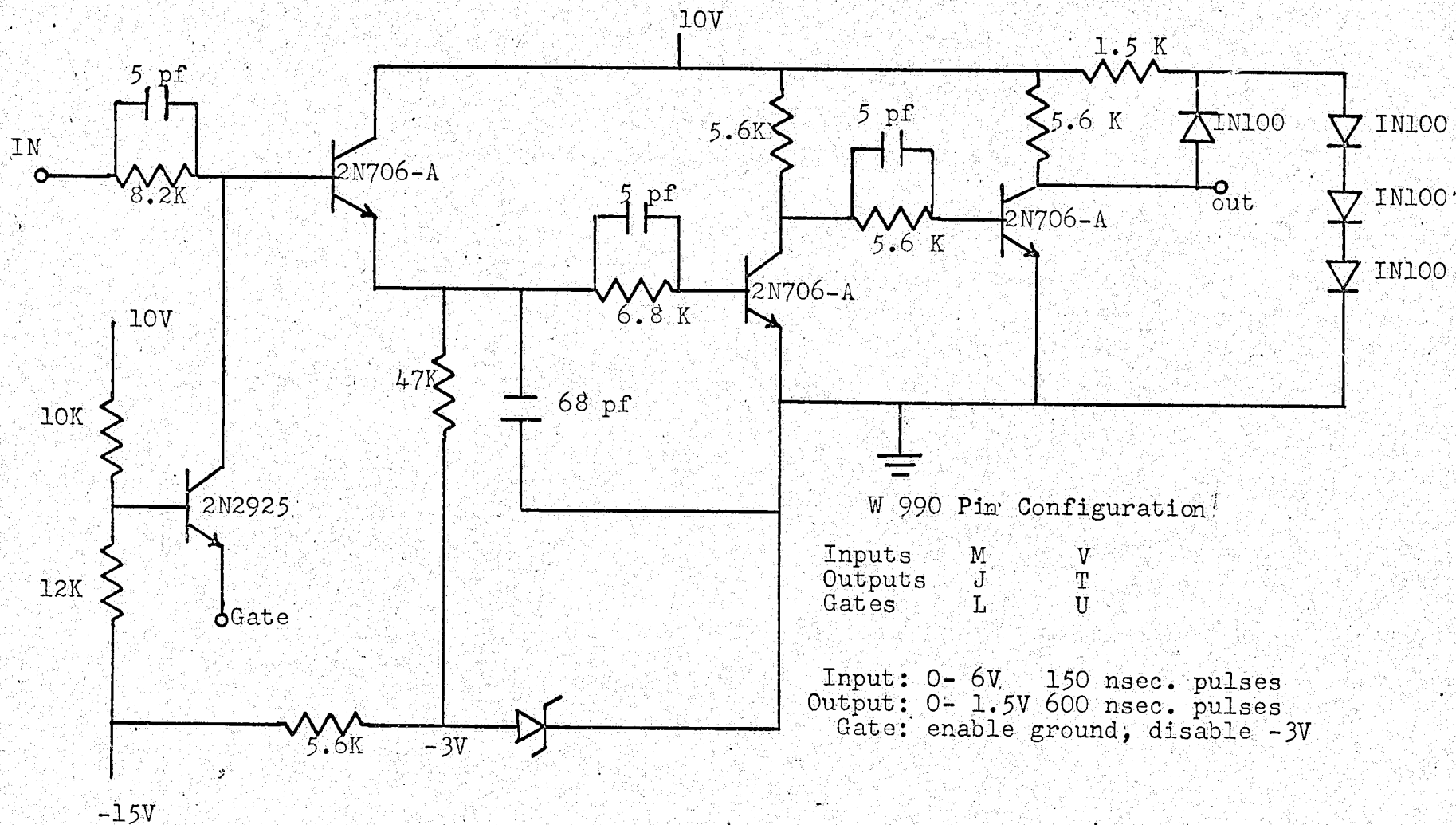
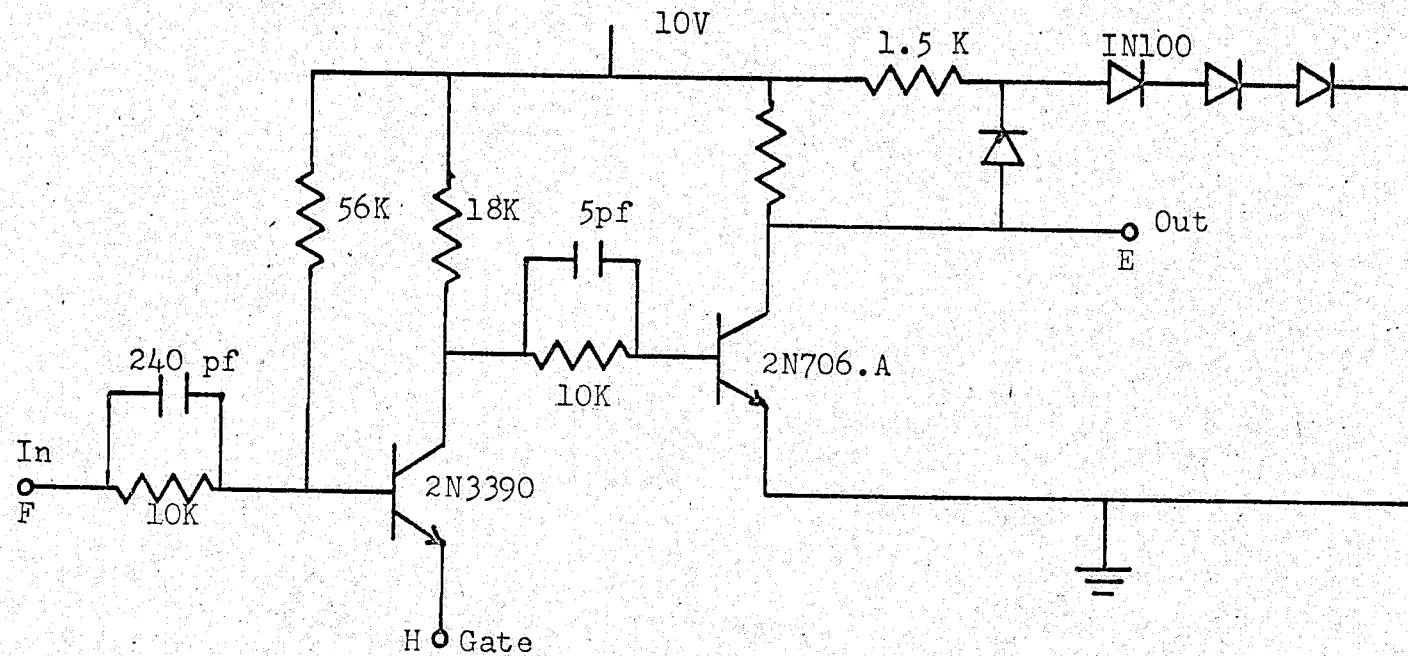


Figure 12. Cosmic - $C_{\mu}L$ Gated Converter



Input: -3V - 0V 100 nsec pulses
 Output: 0V - 1.5V 200 nsec pulses
 Gate: Ground enable, -3V disable

Figure 13. Gated Clock Converter

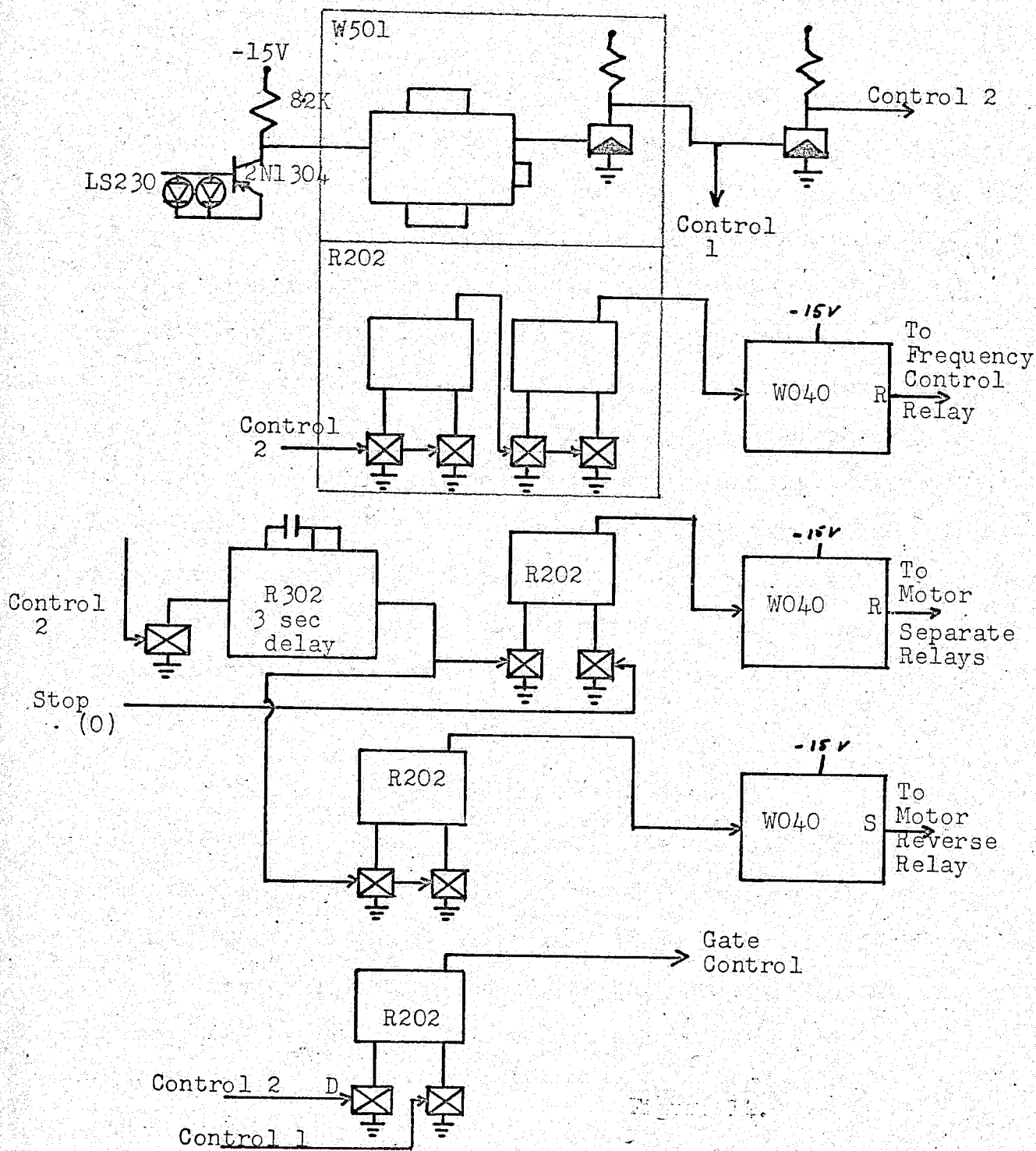


Figure 14. Control System Electronics

system over small light bulbs. The position of these photocells is adjusted so that if either cell is cut off from its light source the level at the collector of the transistor drops far enough to trigger the Schmitt Trigger and supply a pulse for the electronic controls. These photocells are used to indicate the endpoint of the rider traversal simply by mounting small metal strips on the transport which will slide between the photocell and its light source. The endpoint position can then be adjusted by adjusting the position of these strips. This method of endpoint indication is far superior to the usual microswitch arrangement as no physical contact is required. The inverter on the output of the Schmitt Trigger provides a D.E.C. pulse (-3 volts to ground) when the photocell is opened to the light. This provides a starting point indication.

The "gate control" flip flop closes all the gates to the scalers when one of the photocells is cut off and opens them again only when the transport has moved far enough to open the photocell to its light source again. This automatically allows time for the transport to accelerate to constant velocity before any counting is done as the motor is allowed to overdrive the cutoff point for 3 seconds by the R302 delay before the "motor separate" relays are opened. The state of the "motor reverse" relay is changed simultaneously with opening of the "separate" relays thereby causing the motor to drive in the reverse direction when power is restored. When the scaler printout has been

completed as indicated by the "Stop (0)" output returning to ground the motor separate relays are closed and the transport is driven in the opposite direction.

The control relay wiring which is shown in Fig. 15 is much the same as that used by Wells. The oscillator which is to change the driving frequency of the motor and thus its velocity is a Hewlett Packard 421 A pushbutton model. The change in frequency is effected by pushing two preselected buttons with small solenoids activated through the "frequency control" relay (Fig. 15b). The state of this relay is changed at every second endpoint indication via the R202 flip flops. This provides the required velocity pattern of $V_1 - V_1 V_2 - V_2$ etc. This particular part of the control electronics was not used in the present work as no shift measurements were actually made, however the system was set up and made operational.

3:6 Scaler Clearing

At the end of each printout all the scalers were cleared by the circuit in Fig. 16. This circuit is activated by the "0" output of the motor separate flip flop which gives a -3 volt to ground pulse when the Stop (0) signal comes indicating the end of the printout. The four diodes on the base of the output transistor are used to clamp the clearing pin at 1.5 volts to prevent any overvoltage at this point. The circuit as shown was mounted physically near the scalers so that the scaler power supply could be used.

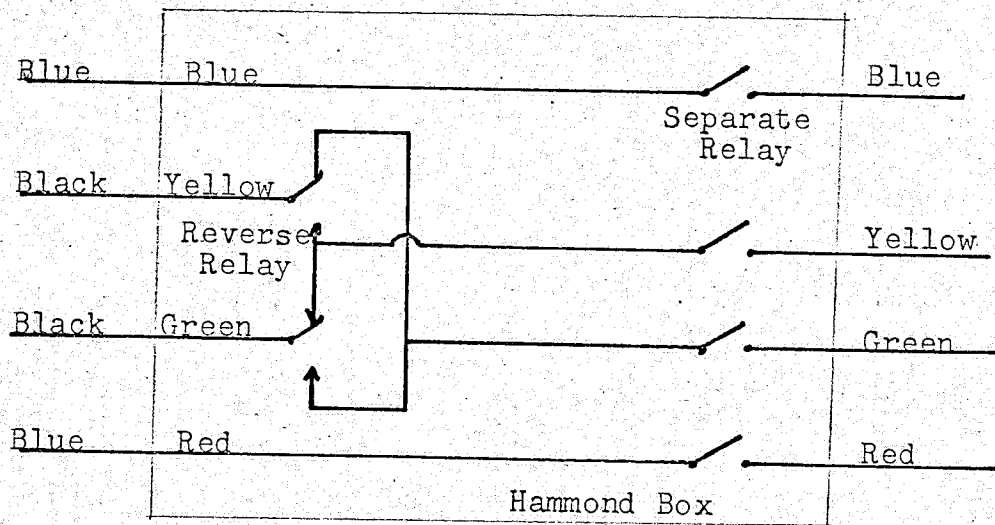


Figure 15 (a). Motor Control Relay Wiring

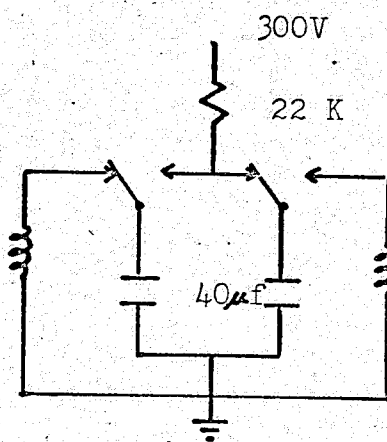


Figure 15 (b). Frequency Control Relay Wiring

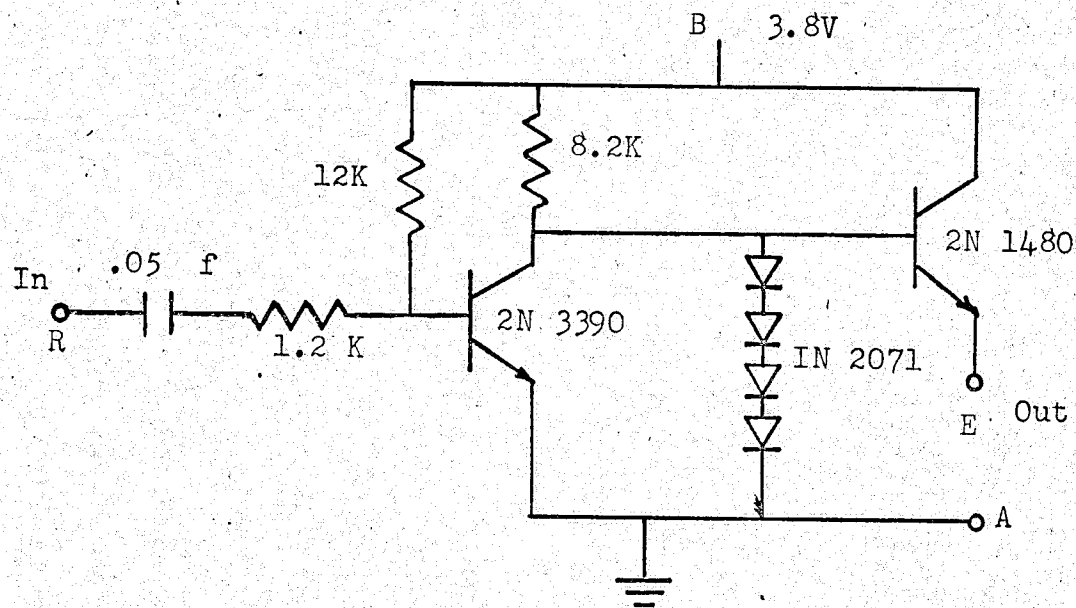


Figure 16. Scaler Clearing Circuit

CHAPTER IV

VELOCITY MONITORING SYSTEM

The laser interferometer used by Wells was felt to be an excellent method of monitoring the velocity of the source/absorber transport system and was used throughout this experiment. Some refinements were found to be necessary to obtain realistic velocity measurements and will be summarized in this section.

The Spectra Physics model 130 gas laser used for the interferometer was found to have beam intensity fluctuations of 60 and 120 c.p.s. These fluctuations were less than 5% of the velocity signal when the interferometer was well adjusted (i.e. the mirrors were perfectly parallel and the central fringe covered the whole of the laser beam) and the laser intensity was set in the medium range. At higher and lower intensities the 120 c.p.s., noise became quite large. This noise problem made it necessary to adjust the interferometer very well and to operate the transport system only in regions where the interferometer remained in adjustment. When the interferometer came out of adjustment so that several lines were visible over the laser beam the signal decreased to the noise level and made meaningful velocity measurement impossible.

It was found that vibrations of the laser relative to the mirrors would produce a signal on the photocell due to a shift

in the position of the interference pattern. This problem was eliminated by mounting the laser close to the mirrors on the same piece of steel as the transport system which effectively tied the two structures together.

The photo resistor used by Wells was found to be wholly inadequate for our purposes as it had an extremely poor frequency response which limited the range of velocities which could be measured. This problem was further enhanced by the laser noise which soon became comparable to the signal as the velocity was increased. Three other photo cells were tried to overcome this problem

- (1) LS 230 photo voltaic
- (2) H 38 photo diode
- (3) LS 400 photo diode

All the above photocells had excellent frequency responses but varied greatly in sensitivity. The LS 230 was found to be sensitive in the infrared region but insensitive to the 6300 \AA radiation of the laser. The H-38 and LS 400 photo diode were found to be much more sensitive to the laser light and both were found satisfactory for our application. The LS 400 was the more sensitive of the two and was used for most of the measurements in this experiment.

The sensitivity of the LS 400 diode made it possible to collimate the laser beam by an eight thou hole placed directly

in front of the diode. This made the signal to noise ratio much less sensitive to the adjustment of the interferometer as only a small portion of the interference pattern was being observed by the photocell. This feature greatly increased the length of movement allowed by the transport system especially for the air bearing where the interferometer adjustment was found to change with position.

The circuit diagram for the velocity monitoring system is shown in Fig. 17. In this circuit the 3.9 K resistor in the Darlington amplifier was chosen such that the gain of the amplifier was high enough that the full swing of the photo diode with the 8 thou collimator would trigger the tunnel diode but low enough that the laser noise would not exceed the hysteresis of the tunnel diode thus causing many spurious pulses when the switching point was reached. The output of this circuit is a positive 1.5 volt pulse with a very fast rising leading edge required to trigger the micrologic scalars. The circuit as shown works very well and gives an almost unambiguous correspondence between the behavior of the interference pattern and the signal output. The only ambiguity is in the pulse width which will depend on the laser noise and on the d.c. conditions at the input of the Darlington amplifier which are not stabilized in any sophisticated manner. Typical pictures of the output are shown in Fig. 18 and Fig. 22.

CHAPTER V

TRANSPORT SYSTEMS

5:1 Air Track Suspension

It was decided to continue with the basic air track suspension developed by Wells as it had not been proven convincingly that it was unfeasible to remove the troubles encountered with this system. The only major change made was to invert the track and rider so that the center of mass of the rider was below its centre of buoyancy. This made the rider at least statically stable, which was not the case in the original configuration, and allowed the rider to be driven through its centre of mass. This modification did not produce any marked improvement over the previous performance of the system.

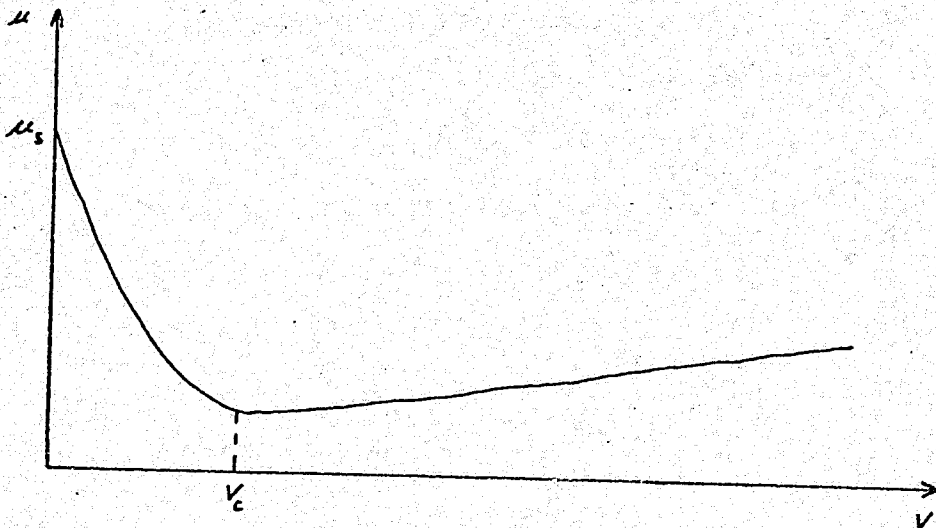
Vibrations transmitted to the suspension system from the floor through the supporting structure were studied using an uncalibrated geophone and a high gain type 551 scope. It was found that floor vibrations were especially large at 60 and 120 c.p.s. and that the isolating structure used by Wells amplified vibration at these frequencies and gave effective isolation only for shock inputs. Vibration measurements were made with the same geophone and scope at various points in the building. It was found that floor vibrations were down by a factor of 10 from the original position in the basement optics laboratory and the equipment was moved to this position.

A vibration isolating table was constructed for the suspension by glueing together with contact cement five layers of 5/16" Isomode rubber to form four rubber mounts each of 3.0 square inch area. These were used to support a wooden platform which was loaded with concrete blocks and a 54"x18"x $\frac{3}{4}$ " sheet of steel such that each mount was supporting approximately fifty pounds per square inch. According to the curves supplied by the isomode manufacturers five layers of 5/16" rubber with the above loading should provide isolation to frequencies above 8.2 c.p.s. and have a natural frequency of 5.8 c.p.s. It was found that for the above structure the natural frequency was approximately 16 c.p.s. and isolation was provided above 20 c.p.s. This support was considered to be adequate as vibration levels were small in comparison to those in the previous support and a more elaborate system would be expected to give only small improvements and could become very costly.

The air track suspension was mounted on the steel sheet of the above table and except for the case in which the air was off the velocity instabilities were found to be the same as encountered previously. In the air off case there were only small variations in the fringe pattern, less than $\frac{1}{2}$ fringe when observed visually, which indicated that the vibration level had been substantially reduced and that these vibrations were not directly the cause of the velocity fluctuations. The fact that the velocity instabilities remained essentially the same even

though floor vibrations were greatly reduced indicates that the instabilities are not induced by these external vibrations. It was felt therefore that the velocity instabilities were due to either the drive mechanism or the frictional properties of the track and rider.

The frictional properties of steel on steel were found in references 13,14,15,16,17. The thesis by Roderick Cameron was particularly interesting as his results were substantially like the velocity oscillations we were observing over the same velocity range. This suggested that we had steel on steel contact, which was verified by measuring the resistance between the track and rider with the air on, and that we were observing the slip stick process associated with steel over steel motion. This slip stick process occurs for velocities below some critical velocity where the coefficient of friction increases with decreasing velocity, i.e.



Above this critical velocity the motion becomes much more smooth and oscillations as observed for lower velocities are not in evidence. This effect was observed with our system by driving the rider at a much higher velocity and observing the decrease in the amplitude of the velocity fluctuations. There are three things that can be done to decrease the amplitude of oscillations due to the slip stick process

- (1) Increase the velocity above the critical velocity
- (2) Decrease the ratio K/w where K is the stiffness of the driving suspension and w is the normal weight between the track and rider
- (3) Introduce damping into the system.

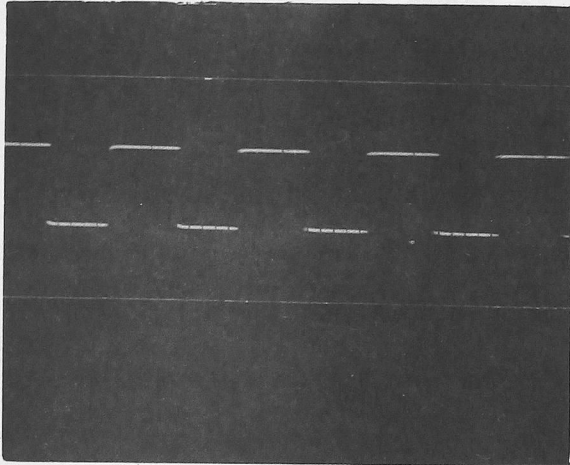
The first of these could not be done in the present application as velocities of interest were well below the critical velocity. The stiffness of the driving pulleys and drive attachment structure was increased as much as possible without a complete redesign of the drive mechanism. This had no observable effect on the velocity fluctuations. The value of w was set by the hydrodynamic stability of the rider as at airflow rates which would float the rider clear of the track, thus reducing w to zero, the rider became unstable and oscillated badly. The minimum value of w is thus obtained when the maximum flow rate which does not cause these hydrodynamic instabilities is used. The remaining solutions are then to eliminate the metal to metal contact or to introduce sufficient damping.

It was felt that a more viscous fluid would provide some damping to the system so a constant head recirculating oil system was constructed to replace the air supply. This oil floatation gave very little improvement over the air system. The frequency of the oscillations with the rider floating but at rest was substantially reduced but they were of equally large amplitude. The velocity fluctuations with the rider in motion were found to be essentially the same as with the air floatation. It was found to be necessary to reduce the oil flow until the track and rider were in contact to eliminate the high amplitude oscillations present when the rider was floating. We were then again observing the slip stick process of steel on steel and any damping caused by the oil was not sufficient to affect the oscillations.

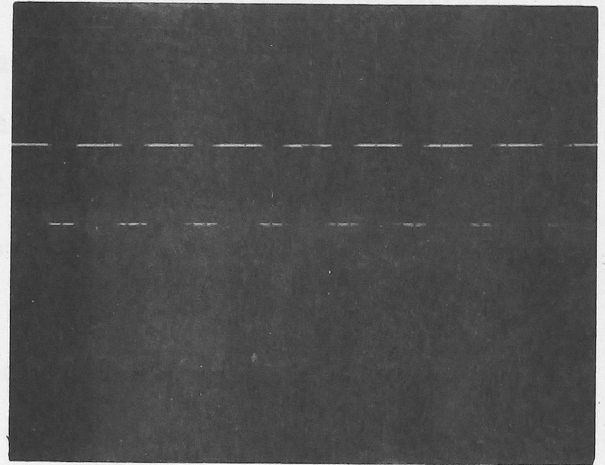
To eliminate the steel on steel contact small teflon tabs of approximately $1/64$ " thickness were attached to the eight corners of the rider. This completely eliminated the metal to metal contact when the rider was placed in the track. The oil floatation system was maintained to support the bulk of the weight of the rider and to lubricate the teflon on steel contact points. This modification produced a marked improvement in the performance of the suspension system. Fig. 18 shows typical pictures of the velocity measurement system output for various velocities. The top two pictures were taken at $1/50$ and $1/25$ sec. time settings on the camera and represent 10 and 4 traces of the scope

A

B



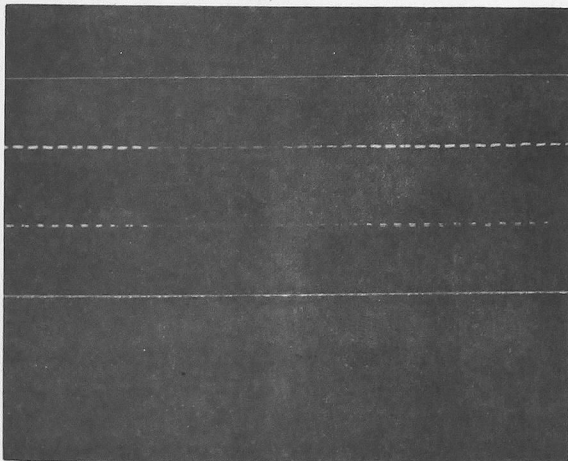
V 0.75 mm/sec
Sweep 0.2 ms/cm



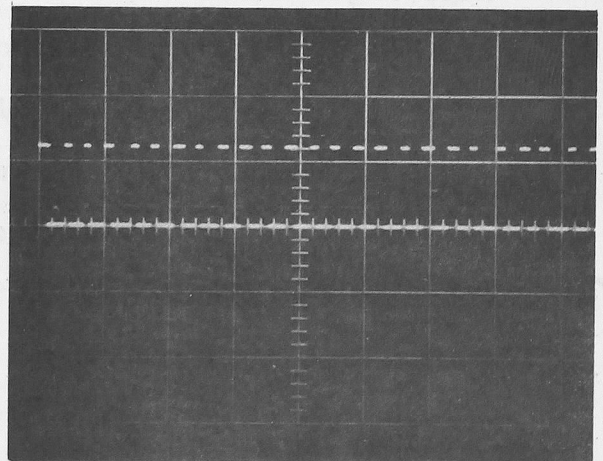
V 0.28 mm/sec
Sweep 1.0 ms/cm

C

D



V 0.13 mm/sec
Sweep 10 msec/cm



V .045 mm/sec
Sweep 20 ms/cm

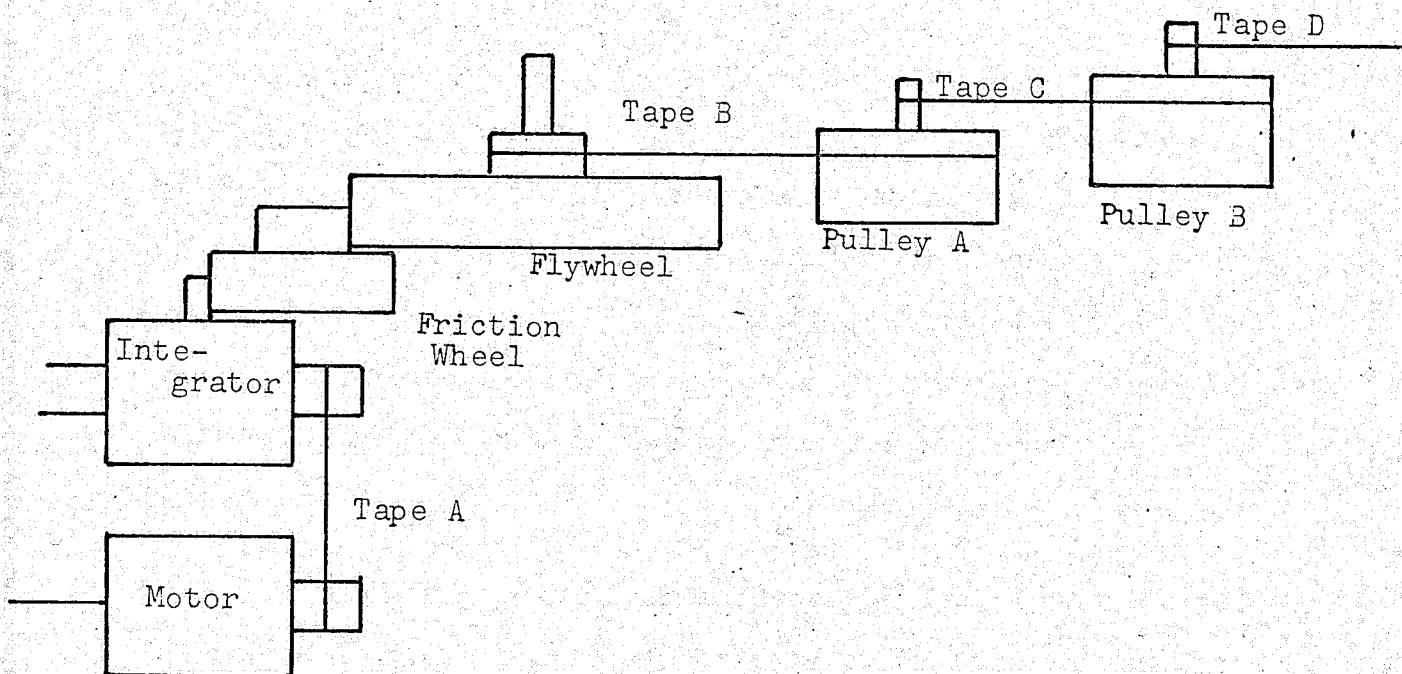
Figure 18

respectively. The bottom two pictures were taken manually and represent a single sweep of the scope. The large frequency fluctuations observed by Wells are not present in these pictures however there are definitely some fluctuations which indicate the presence of velocity instabilities. The magnitude of these frequency or velocity fluctuations depends upon the position of the rider which would indicate irregularities in the track surface or in the steel tape which drives the rider. Other irregularities in the velocity could be due either to variations in the friction coefficient between the track and rider or to the actual driving system.

5:2 Mechanical Drive System I

The first mechanical drive system, Fig. 19, used in this experiment was very similar to that used by Wells. The motor, ball disk integrator, friction drive wheel and flywheel form one unit of the drive and are mounted on an angle iron framework supported by cement blocks. This unit gives a continuously variable rotational velocity of the flywheel between 0 and 10 r.p.m. The flywheel is the same as that used by Wells and is used to damp out any velocity fluctuations introduced by the motor and ball disk integrator. The performance of this unit was roughly checked by mounting an aluminum wheel with 360 equally spaced slots around its circumference on the flywheel axis and monitoring the rate at which the slots passed a fixed point with a photo cell. The motor speed was also checked by

Mechanical Drive System I



Motor: Bodine Electric Co. Cat. 2270

4 Lead Synchronous Capacitor A.C. Motor

115V, 60 cps, 1/75 H.P. 1800 R.P.M., Output Dia. 0.5"

Integrator: Librascope Inc. Part No. 879258 - 1

Ball Disk Integrator, Output 0-2x Input

Input Diameter 0.378" Output Diameter 0.25"

Flywheel: Rek-O-Kut Model G.1 Broadcast Turntable

Input Diameter 15.5" Output Diameter 1.994"

Friction Wheel: Rubber turntable Drive Wheel

Input Diameter 1.445" Output Diameter 0.609"

Pulley A: Roberts Capstan Pulley

Input Diameter 2.105" Output Diameter 0.479"

Pulley B: Roberts Capstan Pulley

Input Diameter 3.335" Output Diameter 0.478"

Tape A: Fabric 17" x 1/2" x 12 M.l.

Tapes B, C: Kinelogic, Corp. Seamless Mylar Belts

Length 43.075" Width .3125" Thickness 0.005"

Tape D: Steel 54" x 50 M.l x 3 M. 1

Figure 19

illuminating the moving shaft with a stroboscope. Neither of the above checks showed any indication of velocity fluctuations.

The rider was driven by an endless steel tape which was driven by the second capstan pulley, pulley B, mounted at one end of the track. The tape was attached to the centre of the rider and tensioned by an adjustable tail pulley at the opposite end of the track. The position of attachment of the tape to the rider was made adjustable in the plane perpendicular to the steel tape so that the optimum driving point could be found.

The alignment of the capstan pulley, the drive point and the tail pulley was found to be very critical, therefore the track and rider assembly was mounted on a platform which was adjustable in height and position, relative to the two pulleys, by means of screws at the four corners. The height of the platform was chosen first and the platform levelled. The laser was then levelled and adjusted so that the beam was bisected by both the head and tail pulleys of the drive. The track was then aligned by placing a lucite block with a central scribed line at each end of the track and adjusting the platform position until the laser beam was bisected by both these lines. One centering block was then removed and the other used at each end alternatively for the final adjustment. The rider was then placed in position and the attachment point adjusted so that it was central in the laser beam. This procedure was repeated several times to

ensure that the alignment was as precise as possible.

The vertical alignment of the head and tail pulleys so that the tape would not "walk" up and down the pulleys was found to be very difficult and was overcome by putting a small groove in the tailpulley and replacing the steel tape with the minimum length of copper wire at this position. The copper wire was attached to the tape with solder. The only problem encountered with this procedure was that the copper tended to stretch when under tension and the tailpulley had to be adjusted periodically to correct for this.

The first capstan pulley, pulley A, was mounted on cement blocks separate from both the motor drive unit and the suspension table. This pulley served the function of reducing the velocity of the drive and isolating the vibrations in the drive unit, caused by the motor, from the suspension system. This isolation worked very well as the supporting structure of the drive unit could be disturbed quite drastically before any effect was observed in the output of the velocity monitoring system.

The drive system as shown gives a velocity of the rider which is continuously adjustable between 0 and 1.0 mm/sec. The maximum range over which the rider could be driven was 25 mm, however only 5 to 10 mm of this was used as the adjustment of the velocity measurement system was much easier for a small range

and the position of best velocity stability could be chosen.

5:3 Leadscrew Suspension

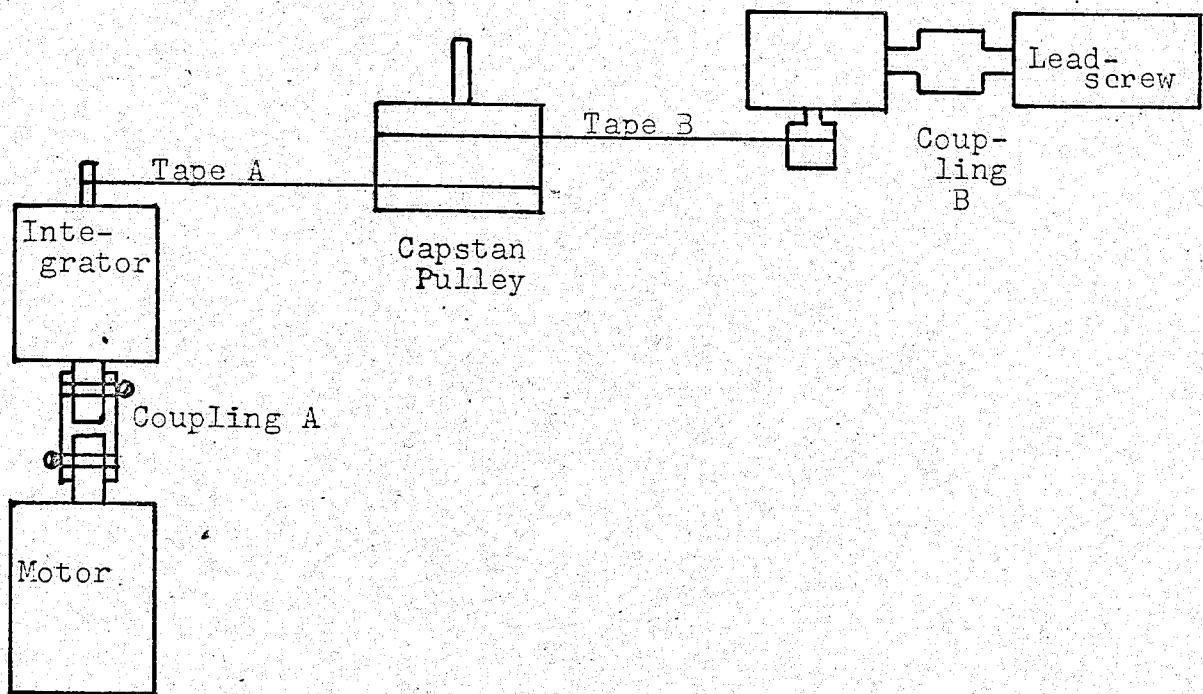
The second suspension system used in this work was a precision leadscrew and carriage which was purchased from Gaertner Scientific Corporation in the form of a M301 micrometer slide. Details of this unit are given in Fig. 20 and 21. The aluminum structure holding the source/absorber and moving mirror was bolted to the slide through the threaded hole provided for microscope mounting. Except for this mounting structure the micrometer slide provided a complete suspension system of the conventional leadscrew form.

5:4 Mechanical Drive System II

The drive system used for this second suspension is shown diagrammatically in Fig. 20. The 12:1 reduction gear and the micrometer slide formed a single unit which was mounted on a $\frac{1}{4}$ " aluminum plate which in turn was screwed to the steel plate on the vibrator isolation table used for the first suspension. It was necessary to take great care in the alignment of the output shaft of the reduction gear and the input shaft of the micrometer slide as no binding due to misalignment could be tolerated at this point. These shafts were connected together using a T 11-6ⁱ neoprene flexible coupling. The input shaft of the re-

ⁱP.I.C.

Mechanical Drive System II



Motor: Bodine Electric Co. Cat. 2270
 4 Lead Synchronous Capacitor A.C. Motor
 115V, 60 cps, 1/75 H.P. 1800 R.P.M.
 Integrator: Librascope Inc. Part No. 879258-1
 Ball Disk Integrator Output 0-2x Input
 Input Diameter 0.378" Output Diameter 0.25"
 Tapes A & B: Kinelogic Corporation Seamless Mylar Belts
 Length 43.075" Width 0.3125 Thickness 0.005"
 Capstan Pulley: Input Diameter 3.50" Output Diameter 3.335"
 Roberts Capstan Pulley
 Reduction: Precision Instrument Corporation 12.5 : 1 Reduction
 Gear
 Leadscrew: Gaertner Scientific Corporation
 Type M-301 Open Micrometer Slide
 Range 5.0 cm Leadscrew Pitch 1 mm

Figure 20

LEADSCREW SUSPENSION

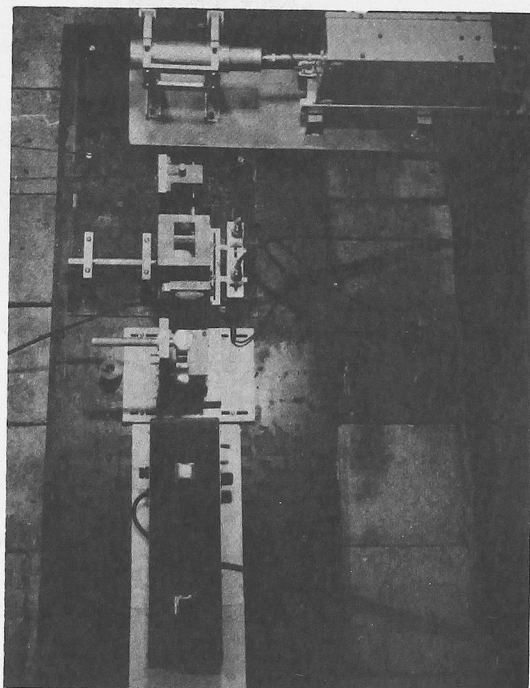


Figure 21. Leadscrew Suspension with velocity monitoring system and detector-preamp combination.

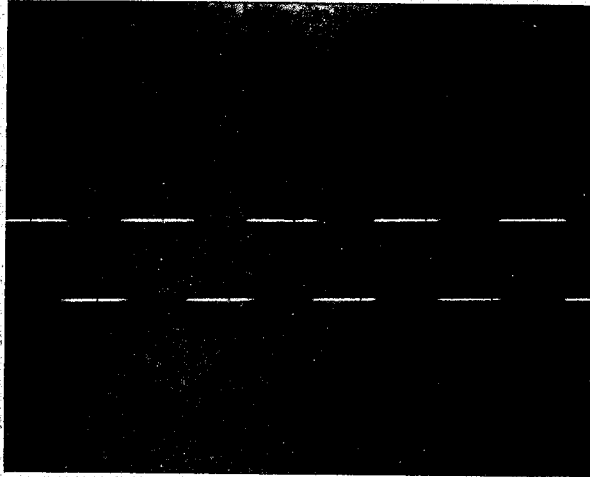
duction gear was fitted with a $\frac{1}{2}$ " brass bushing which was made to be concentric with the shaft to a tolerance of $\pm .005$ ". This bushing was used to improve the wrapping properties of the driving belt, i.e., the mylar belt would not drive the reduction gear through the $\frac{3}{16}$ " shaft.

The capstan pulley was mounted on a cement block stand separate from both the motor assembly and the isolation table. This pulley was used mainly to isolate vibrations induced by the motor from the suspension system and provides only a small amount of speed reduction.

The motor and ball disk integrator from the third part of the mechanical drive. These two units were mounted in an aluminum box with great care taken in the alignment of the connected shafts. A strong piece of rubber hose clamped to each shaft was used as a coupling material. This provides a very rigid coupling of the shafts as the coupling distance is only $\frac{1}{8}$ inch. This unit was also mounted on a cement block stand.

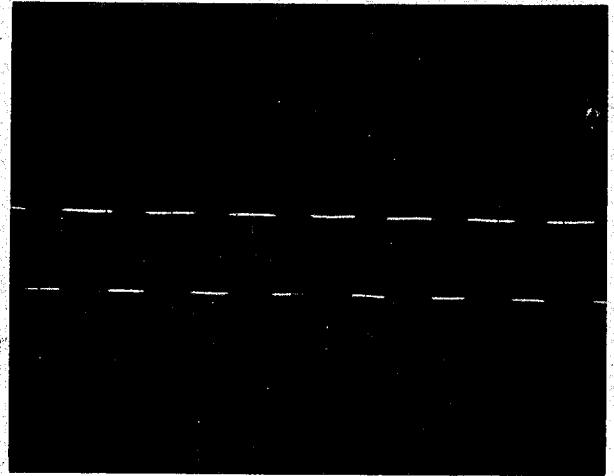
Typical output traces from the velocity monitoring system with the above drive and suspension are shown in Fig. 22. These show that there are still velocity fluctuations present. The velocity is very stable over periods of $\frac{1}{50}$ sec but not stable over periods of 1 sec. which indicates that the velocity fluctuations are of fairly low frequency. The velocity stability seems to be at least comparable to the oil suspension system.

A



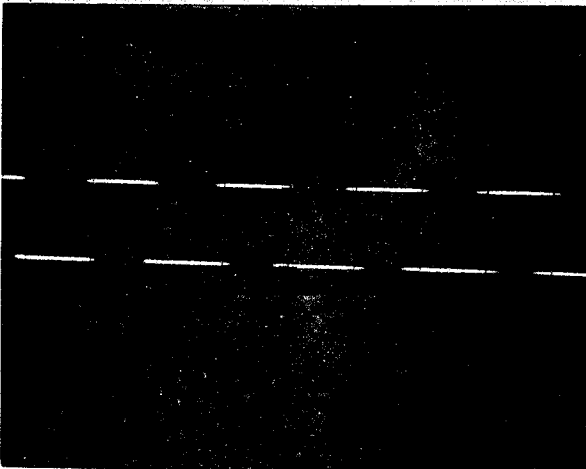
Sweep 0.5 ms/cm
Time 1/50 sec

B



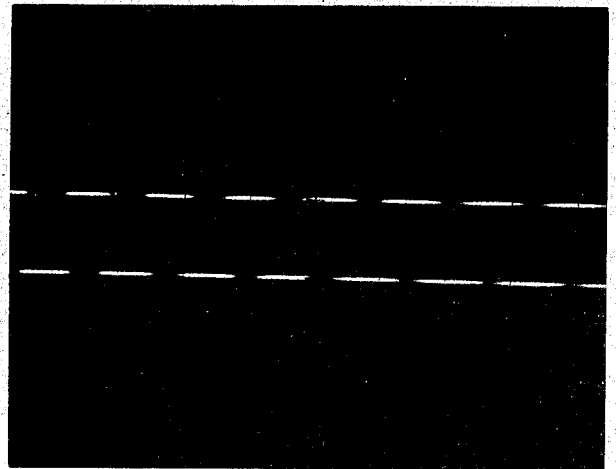
Sweep 2.0 ms/cm
Time 1/50 sec

C



Sweep 0.5 ms/cm
Time 1.0 sec

D



Sweep 2.0 ms/cm
Time 1.0 sec

Figure 22

The above mechanical drive system is considered to be far from ideal. The ball disk integrator in particular is being used beyond its design specifications in this application in both input r.p.m. and output torque. Very low velocities were in fact unattainable as the integrator would not drive the pulley system. This drive also did not utilize the flywheel used in the previous system so that any slippage in the integrator was not mechanically filtered. These undesirable features were necessitated by time and parts available and it is suspected that when these have been designed out of the system the velocity stability will be greatly improved.

The traversal endpoint determination for this second drive system was again alone with LS230 photovoltaic cells. An additional safeguard was built into this system to prevent the leadscrew from being driven hard onto the stop at one end in the event of a failure of the control electronics. The metal structure supporting the two light bulbs was isolated from the common ground of the electronics by thin sheets of mylar. Metal pieces were mounted on the micrometer slide to cut off the light from the photocells at the endpoint position. These were then in electrical contact with the light bulb structure. If the motor was allowed to overdrive one endpoint the framework supporting the photocells over the lights, which is at ground potential electrically, would act as a second endpoint as the metal indicators touching this would ground out one light bulb. The slide

would then oscillate between these two extreme points until it was manually returned to the centre of the two light bulbs.

CHAPTER VI

EXPERIMENTAL RESULTS

6:1 Oil Supported Teflon Bearing Suspension

The velocity output of the oil supported teflon bearing suspension was not exactly constant. However it was decided that sufficient improvement had been made to justify a measurement of the Co^{57} Mossbauer resonance to determine the effect of the observed vibrations on the experimental line shape and width. This measurement gives a means of comparison between the drive constructed here, drives used by other researchers and those sold by commercial concerns. Since there is usually no attempt made at an absolute measurement of vibrational levels, in Mossbauer drive systems this is the only available method of comparison.

The velocity measurement and gate control circuits were checked by replacing the laser interference pattern with a stroboscope and the gamma ray counter with a pulse generator. The equipment was then run as would be done in the experiment. The velocity and count rate measurement obtained in this manner gave an acute test to these circuits as any malfunction would give an obviously absurd answer. The velocities and count rates measured in this fashion were always found to be constant to a degree well within the specifications of the stabilities of the

pulser and stroboscope.

The spectrometer as designed will only automatically cover four velocities so it is necessary to manually change the velocity setting, by adjusting the ball disk integrator, if an entire Mossbauer spectrum is to be taken. Since this manual operation was necessary in any case the motor was driven directly from the main supply and only two points were taken at any one setting. This eliminated the additional complication of the oscillator and amplifier along with the associated control electronics.

The Mossbauer spectra taken with the oil supported suspension are shown in Figures 23, 24 and 26. The source used for the spectra in Figures 23, 24 and 25 was a 99.9% pure Co^{57} electroplated on 0.005 inch Armco iron source obtained from Nuclear Science and Engineering Corporation in 1962. The source strength was originally 4 m.c. but is now approximately 35 μ curies. This weak source strength made the taking of these spectra a very lengthy procedure. The source used for the spectrum in Fig. 26 was the Co^{57} in Pt^{195} mentioned above. The source strength of this was approximately 1 mc at the time of use. The absorber used for all these spectra was a 0.8 mg/cm² enriched iron absorber obtained from N.S.E.C. The experimental arrangement was the usual Mossbauer absorption arrangement with the source moved by the transport system and the absorber mounted between

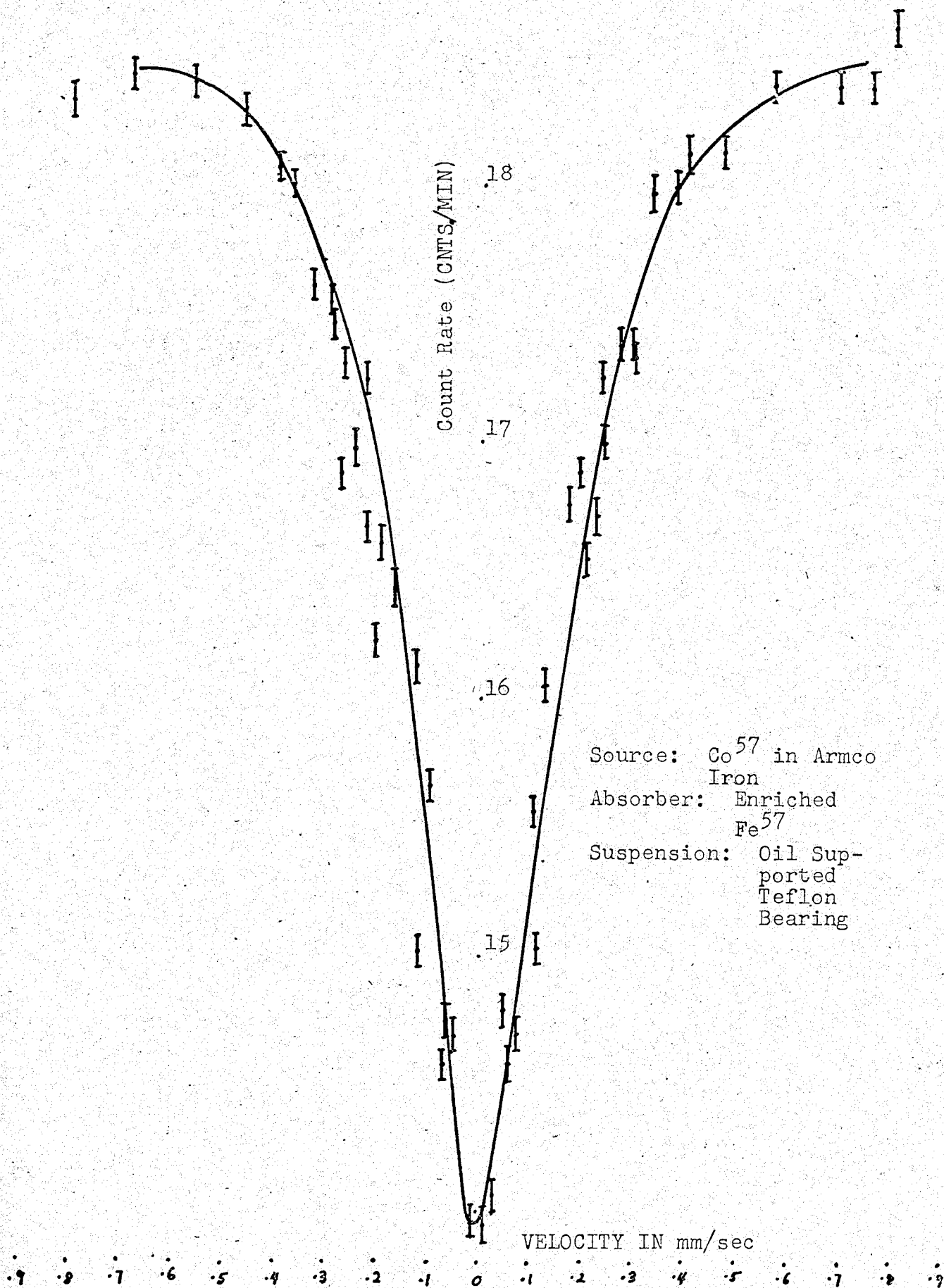


Figure 23

Source: Co^{57} in Armco Iron
Absorber: Enriched Fe^{57}
Suspension: Oil Supported Teflon Bearing

+ Experimental

o Lorentz Fit

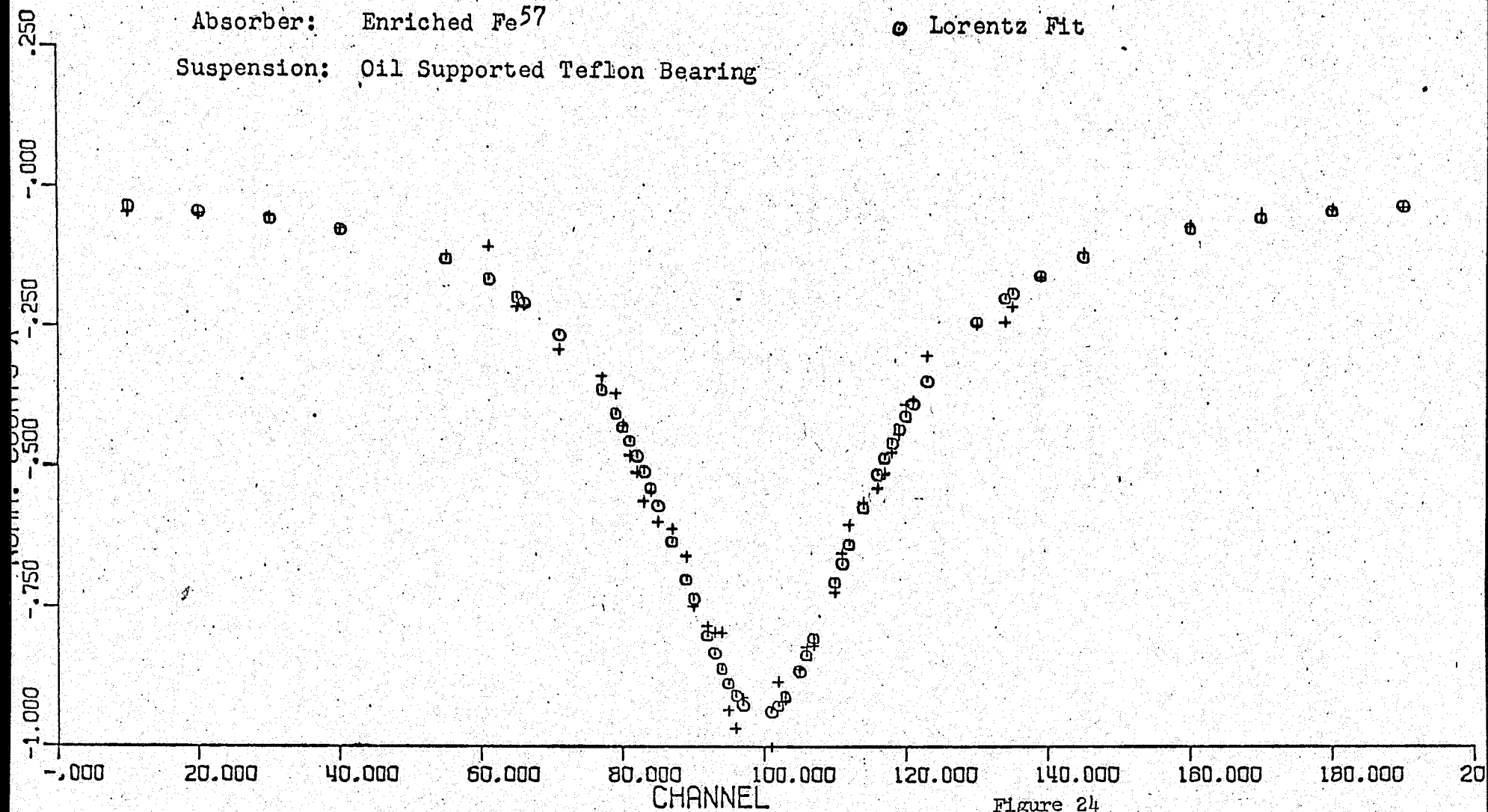


Figure 24

the source and detector. The detector subtended a solid angle of 0.03 steradians. This was kept as low as possible to reduce line broadening due to geometrical effects. i.e. $\Delta V = V(1 - \cos\theta)$

Figure 23 shows the data for the Armco iron source with an "eyeball fit" line drawn through it. The linewidth of this curve is measured to be 3.1 mm/sec. The error bars drawn on the points are obtained only from the counting statistics. Velocities were taken as the calculated value and no estimate of error was made. Velocities and count rates were calculated from the raw data by the use of the computer program (Program I) in Appendix B which was run on the PDP-8 computer. The data for each pair of points was run through the computer and plotted immediately after being taken so that any large discrepancies due to equipment malfunction would be noticed. Some data tapes were run through the computer using a small program which calculated the velocity and count rate for each traversal. The program is much the same as Program I. This provided a check that the averaging procedure used to obtain the velocities was reasonable. It was found that in most cases the calculated velocities for each traversal in a single direction varied by less than 1% over an entire run. This indicates that the velocity average taken is indeed a good velocity measure.

Figure 24 shows the same data with a single least squares fitted Lorentz curve drawn through it. The curve fitting

was done by the computer program (Program II) in Appendix B. This program was written to fit data from a constant acceleration spectrometer and therefore subtracts a parabola from the computed line. In this case the parabola is of no consequence so it is very nearly a straight line. The equation for the parabola is

$$0.135 \times 10^2 + 0.287 \times 10^{-2}x - 0.933 \times 10^{-5}x^2$$

This program was run on the U.B.C. IBM 7090 computer and the plot shown was done by the computer. The velocity in this plot was changed to a channel number such that there are 100 channels per mm/sec. The linewidth calculated from this curve is 3.4 mm/sec. It is obvious from the diagram that the data does not follow a single Lorentzian curve as the lineshape and depth is not well reproduced. This is probably caused by the omission of the satellite peaks on either side of this central resonance. Saturation effects due to the enrichment of the absorber could also cause this discrepancy but these effects are expected to be small. The broadening due to the absorber is given by ²⁶

$$\Gamma(\text{apparent width}) = 2\Gamma'(1 + 0.135t) \quad 0 \leq t \leq 5$$

where

$$t = n f' \sigma_m$$

$$\Gamma' = \text{natural width} \quad 0.095 \text{ mm/sec.}$$

$$n = \text{number of Fe}^{57} \text{ atoms/cm}^2 \text{ in the absorber}$$

$$f' = \text{fraction of recoilless absorptions}$$

$$\sigma_m = \text{effective maximum cross section}$$

We obtain with this absorber that

$$t = 3.70$$

and $\Gamma = 0.286 \text{ mm/sec}$

In this the source is assumed to have no effect therefore the measured width for this source and absorber combination is certainly reasonable.

Figure 25 shows the Mossbauer spectrum taken for the same source and absorber as above on a commercial Mossbauer spectrometer¹ of the constant acceleration type owned by the U.B.C. chemistry department. This shows the central resonance peak and two of the satellite peaks. This data was fitted with three Lorentzians by Program II with a resulting linewidth of 3.1 mm/sec. The fit of the data in this case was very good which substantiates the reasoning for the poor fit of the single Lorentzian. The linewidth here is in good agreement with the eyeball fit to the data obtained with the oil supported teflon bearing. This indicates that vibrations present in this system are at least comparable with the commercial unit. This is only an indication however as the linewidth measured is moderately wide. It is expected, due to the agreement of the two measurements, that the width is determined by the source absorber combination and does not contain equipment broadening.

¹ Technical Measurement Corporation North Haven Conn.
Drive Model 30G
Transducer Model 305

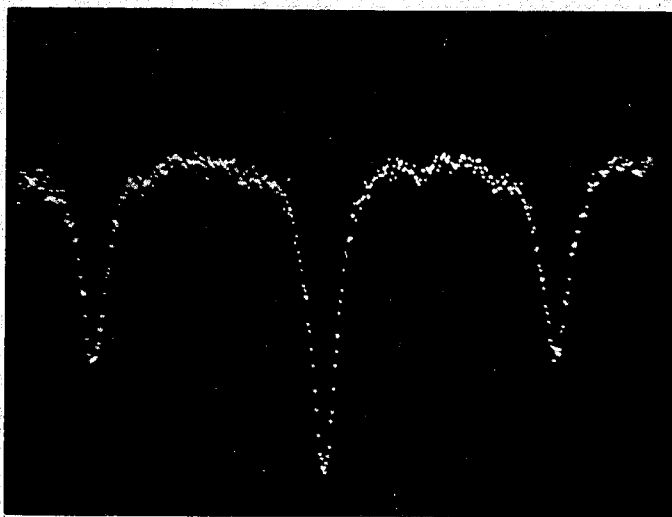


Figure 25. Mossbauer Spectrum for Armco Iron Source vs. Enriched Iron Absorber using Technical Measurement Corporation constant acceleration spectrometer.

The Mossbauer spectrum taken for the Co^{57} in Pt^{195} source with the teflon bearing suspension is shown in Figure 26. This data was taken under the same experimental conditions as above. This source displays only a single line resonance so that only the Zeeman split lines of the absorber are seen and no resonance occurs at zero velocity. The first two lines are shifted from their expected positions at ± 0.8 mm/sec. and appear at $+ 0.5$ mm/sec and at same velocity greater than 1.0 mm/sec in the negative direction. This shift is probably an isomer shift due to the different chemical environment of the source and absorber. Only the line centred at 0.5 mm/sec was observable in its entirety with the present spectrometer. This line is shown in Fig. 26. The second resonance peak was evidenced by a decrease in count-rate at the extremes of the negative velocity end of the spectrum however this is of no consequence here and is not shown. The linewidth measured by an eyeball fit to this data is 0.26 mm/sec. This is much narrower than the linewidth measured for the Armco iron source which indicates that either the vibrations in the system decrease with increasing velocity, which is possible if the stick slip process is still occurring, or the Armco iron linewidth has little instrument broadening as was suggested above. The latter suggestion is most likely as teflon on steel should not exhibit stick slip. This is borne out by the previous velocity measurement.

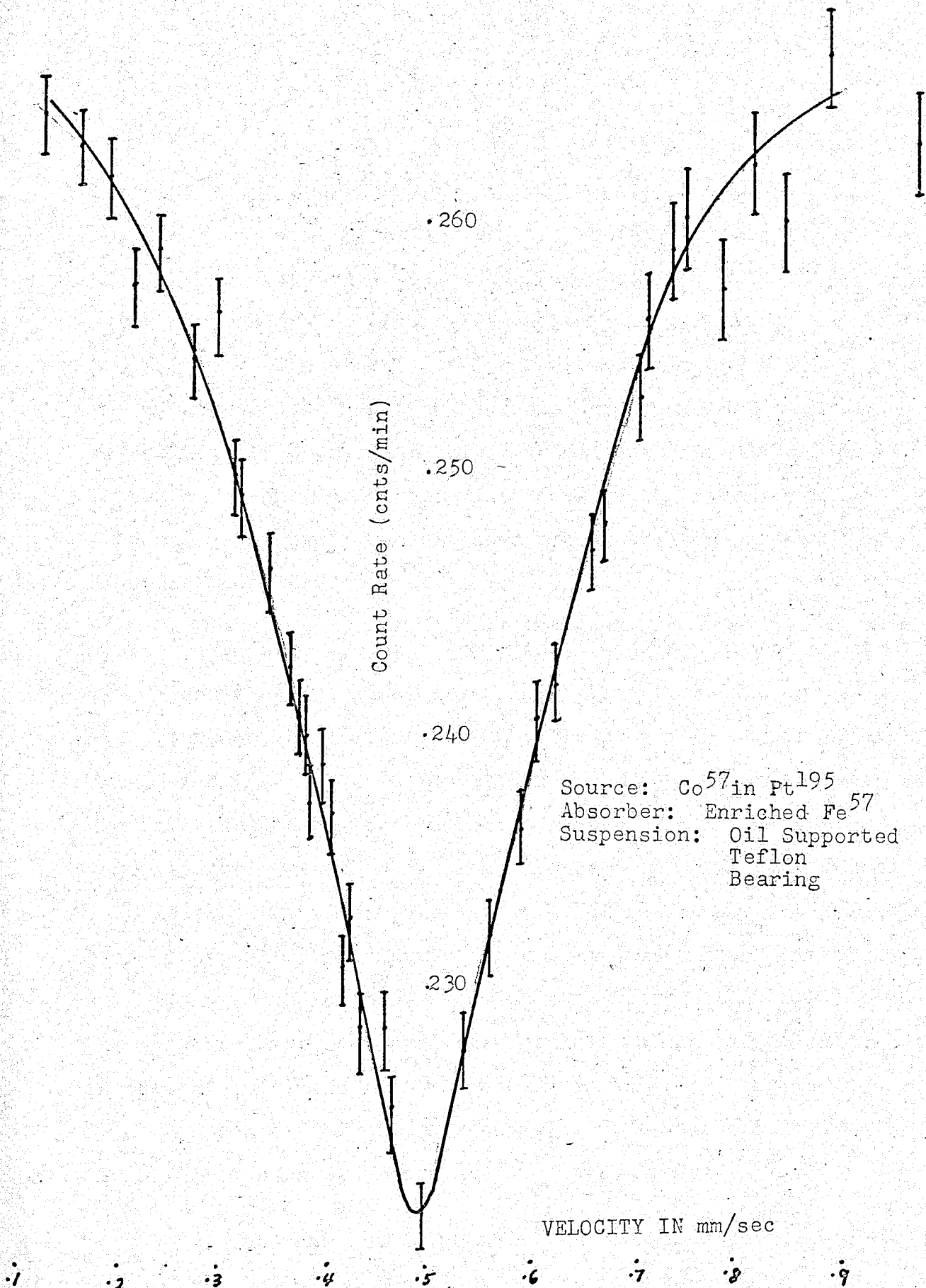


Figure 26

6:2 Leadscrew Suspension

A set of Mossbauer spectra similar to those taken with the oil supported teflon bearing was taken with the leadscrew suspension. This provided a means of comparison for the two systems. The experimental arrangement was the same as above, however the solid angle subtended by the detector was slightly different as evidenced by the count rates observed. In all cases the solid angle was small so that geometrical broadening was negligible. The spectra obtained are shown in Figures 27, 28 and 29.

Figures 27 and 28 show the Armco iron source spectra with eyeball and least squares single Lorentzian fit curves drawn through them. The extreme three points of Figure 27 are considered invalid as it is felt that the counting electronics had drifted suddenly at this point. Some of the previous points were repeated when this discrepancy was found and all produced much lower count rates than before. This was taken as verification of the electronic drift. For this reason four points were added to the data for the Lorentz fit at either end of the resonance to give some realistic measure to the fit at infinite velocity. The linewidths measured from these two curves were 0.31 mm/sec and 0.36 mm/sec respectively. These results are very similar to those above and similar comments apply.

Figure 29 shows the spectrum obtained for the Co^{57} in

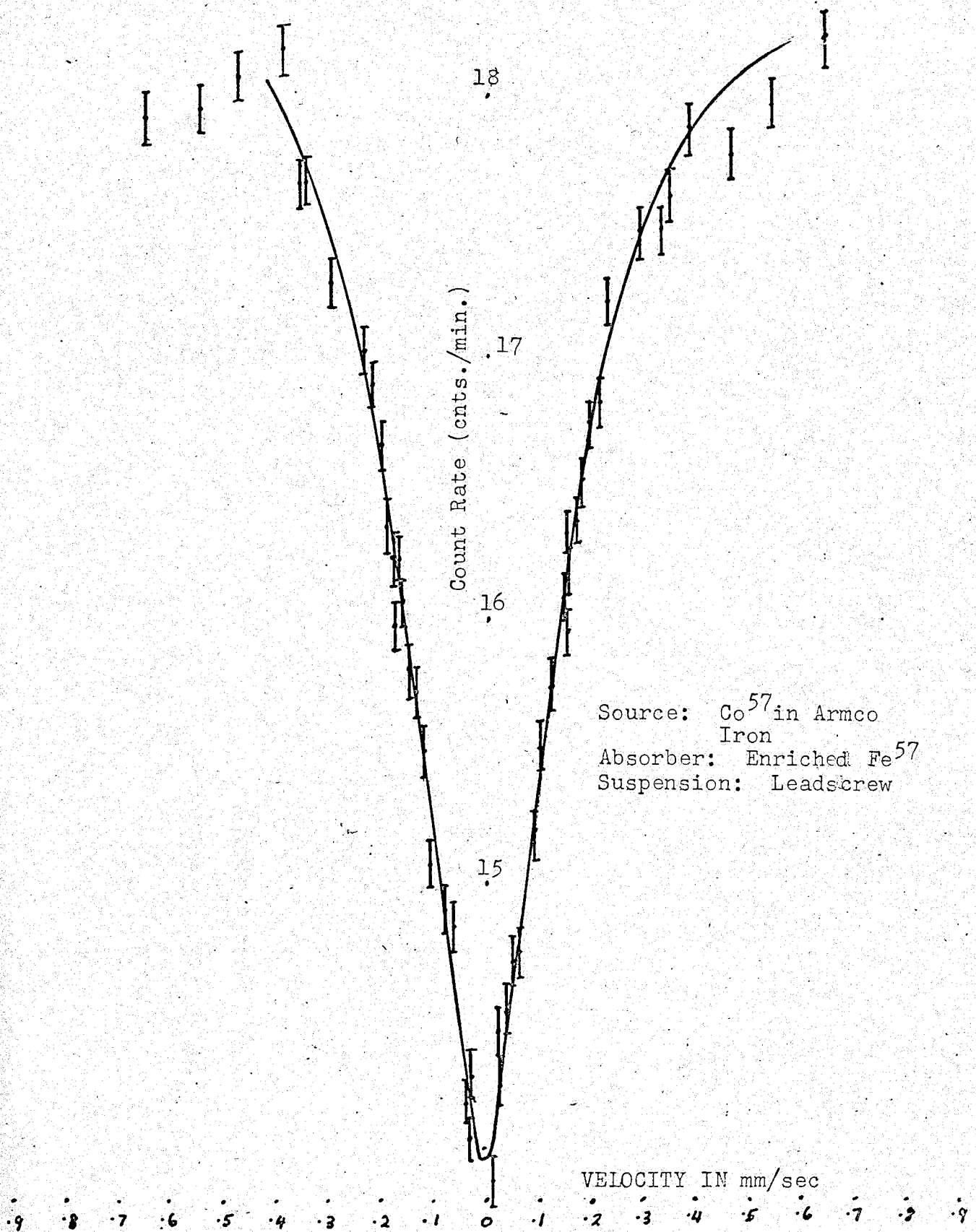


Figure 27

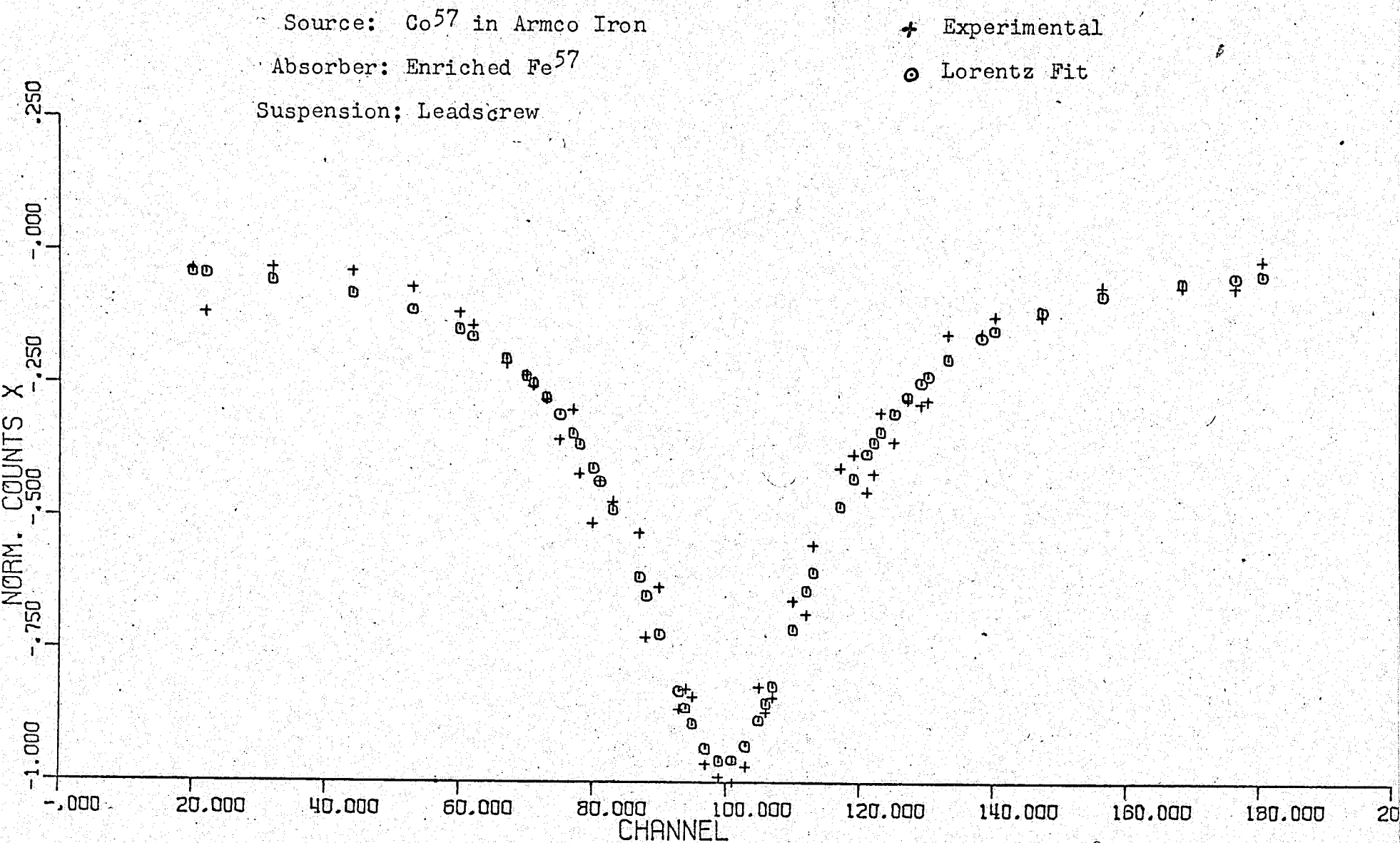


Figure 28

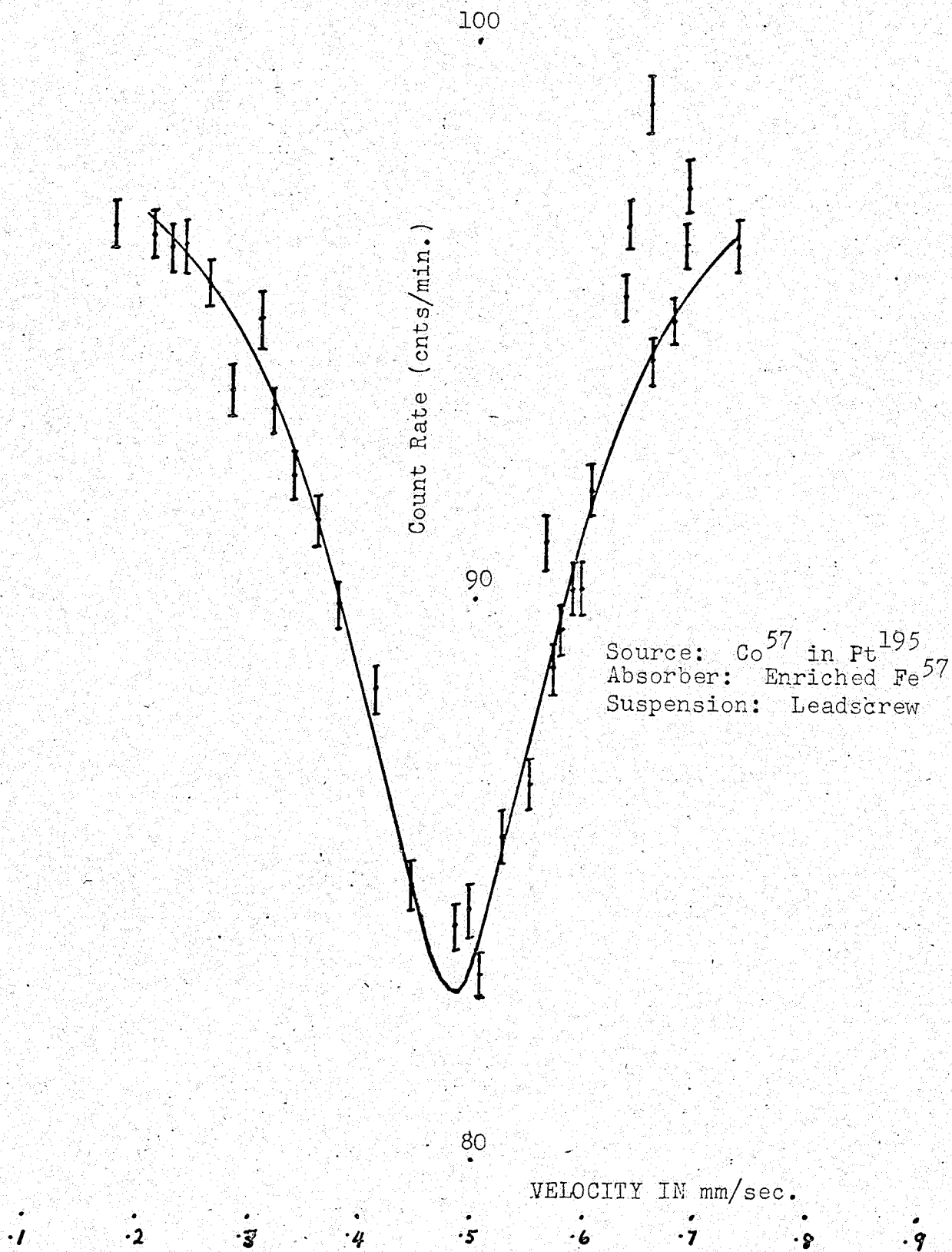
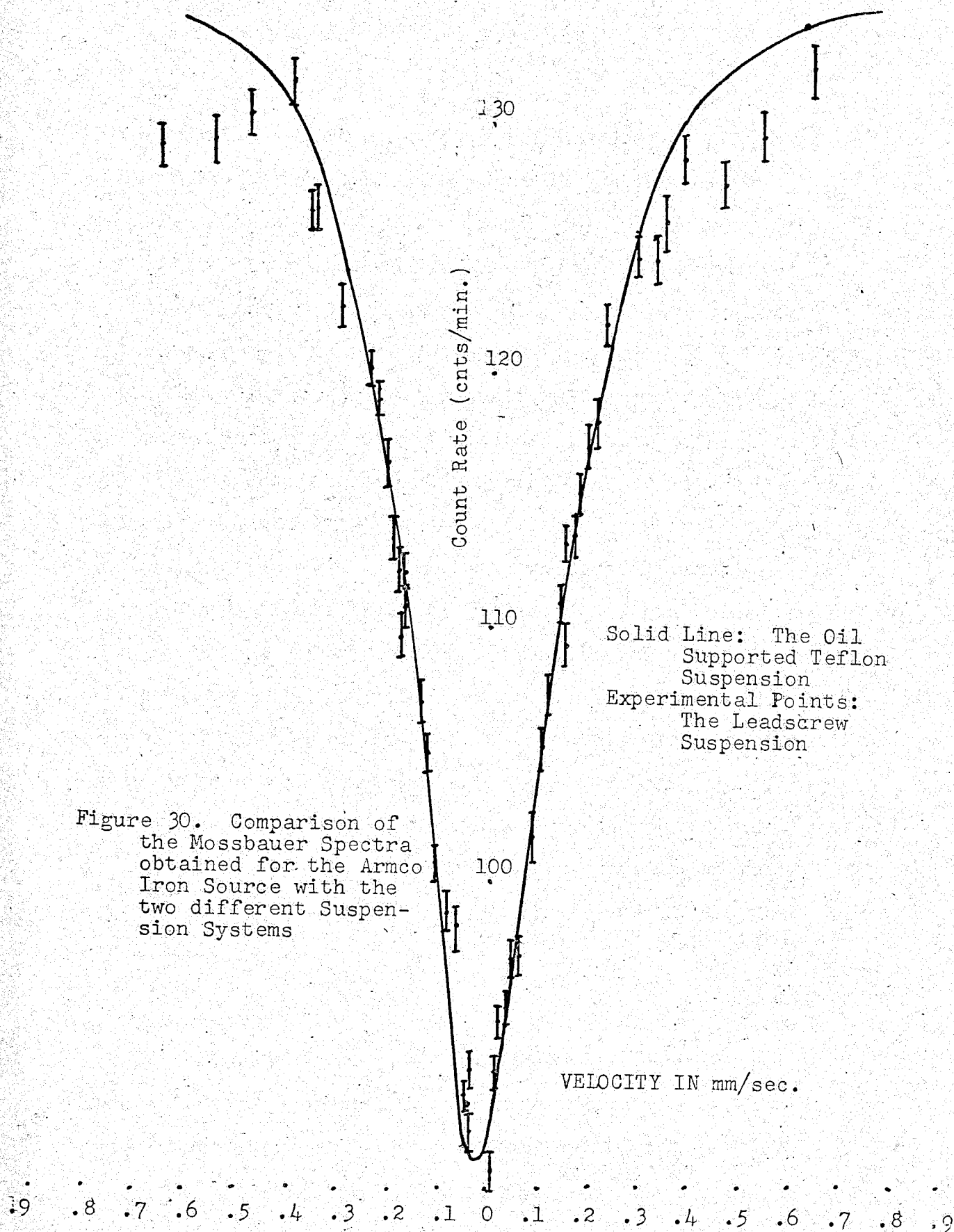


Figure 29



Pt¹⁹⁵ source. Again only the resonant line which was completely observable is plotted. The curve through the data gives a measured linewidth of 0.22 mm/sec. This is quite narrow however the scatter of points at the higher velocities becomes very marked and the curve is asymmetric if the peak position is taken at 0.5 mm/sec as was found previously. This would indicate that either the velocity fluctuations become large enough at these high velocities to affect the lineshape or some malfunction of the scalers developed during the run (i.e. The high velocity points were taken at the end of the run.) The former possibility is not very likely as increased vibrations would tend to broaden the line and the output of the velocity measurement system shows no indication of an increase in velocity fluctuations. The latter point was not checked immediately as the points fell sufficiently close to the expected curve that the large scatter was overlooked in the preliminary analysis. No malfunction was discovered when the scaling units were checked at a later date. The spectrum was not repeated as the velocity range involved is not of interest in the experiment under consideration.

6:3 Comparison

The Mossbauer resonant spectra obtained for the Armco iron source and enriched iron absorber with the two suspension systems used here are plotted on the same scale in Fig. 30. The line drawn in this figure is the "eyeball" fit to the data

obtained with the oil supported teflon steel bearing suspension. The points with error bars are the data points obtained with the leadscrew suspension. We see from this that, except for the six points which were discarded because of electronic drift, these sets of data are in excellent agreement. This measurement of the linewidth of this source and absorber combination gives no means of choice between the two suspension systems as there is no instrument broadening evidenced in either case. A better comparison of the two systems by this means could be done only with a source and absorber combination which display a narrower linewidth, preferably as close to the natural linewidth of Co^{57} as possible.

The output of the velocity monitoring system seems to have approximately the same magnitude fluctuations for the two suspension systems. This is of course a qualitative comparison as no quantitative measures of the fluctuation were taken which were felt to have any accurate significance. The pulse width fluctuation was the same for both systems however as mentioned above this is an ambiguous determination of the velocity fluctuation. The frequency of the pulses was measured with an H.P. Model (5251A) frequency meter. This required a sample time of 1 or 10 sec., depending on the velocity measured, which is longer than the period of the frequency fluctuations as indicated above and therefore the measurement gives only an average frequency. The variation of this frequency measurement was about 2%.

2% for each of the drive systems however it is not clear that this is a meaningful comparative measurement except of the gross stability properties.

For experimental convenience the leadscrew is much superior to the oil supported suspension. This is evidenced mostly in three properties.

(1) Mirror Adjustment -- The adjustment of the moving mirror on the oil supported system was found to change with the position of the rider on the track. This was caused by the change in the manner in which the oil supported the rider from one end of its range to the other. This made it impossible to adjust the interferometer so that velocity measurements can be made over the whole range of movement. This problem was not encountered with the leadscrew drive.

(2) Alignment -- The alignment of the head and tail pulleys of the drive system for the oil supported suspension was found to be very difficult and critical. The leadscrew and output shaft of the reduction gear also had to be carefully aligned however this was done to a close approximation by careful machining of the supporting structures and the final adjustment once completed did not have to be repeated as the whole structure was fastened tightly in position.

(3) Oil System -- The recirculating oil system required for the oil supported suspension is in principle very

messy and requires periodic servicing due to dirt particles picked up by the oil. This could be circumvented in part by enclosing the whole system and installing an oil filter. However it is an inconvenient complication not associated with the leadscrew suspension. The oil system has the added disadvantage that the oil pump, which is a necessary part of the system, adds greatly to the background noise in the laboratory which will give acoustic vibrations to the source and absorber. This problem was partially solved by enclosing the pump in a box covered with acoustic tiles. The obvious advantage of the oil supported transport however is that large masses can be added to the rider without appreciably affecting the frictional properties of the track and rider. This consideration becomes very important when the source or absorber on the transport must be temperature controlled, i.e. by placing it in a cryostat.

As mentioned above the velocity fluctuations were essentially the same in magnitude. It must be remembered however that the drive system for the leadscrew suspension was considered very inferior to its counterpart in the oil supported suspension. Although the same ball disk integrator, which is considered to be the most likely source of velocity irregularities in the drive, was in both drive systems the torque requirements in the leadscrew drive were much greater than for the oil suspension drive. It is therefore felt that the leadscrew in fact provides a smoother suspension system than the oil supported teflon bearing.

CHAPTER VII

CONCLUSIONS

The object of this work was to develop a linear drive and electronics system which would be sufficiently precise to enable the performance of the experiment proposed for the measurement of the lifetime of localized vibrational modes in a crystal lattice. The scaling and control system constructed along with the laser interferometer velocity measurement system provide the necessary electronics however similar success was not encountered with the construction of the linear drive.

The air bearing suspension developed by Wells was found to be unfeasible as it was impossible to eliminate the slip-stick induced oscillations caused by the steel on steel contact in the velocity region of interest as the rider could not be floated free from the track without becoming hydrodynamically unstable. This problem could perhaps be overcome by more accurate machining of the track and rider surfaces. However, this is very difficult and expensive with such large surfaces. This suspension, when modified to an oil supported teflon-steel bearing suspension showed a marked improvement over the air bearing as the stick slip process had been removed. However, some velocity fluctuations were obviously present. The measurement of a Co^{57} - Fe^{57} source-absorber pair linewidth showed no instrument broadening greater than that of a commercial

constant acceleration spectrometer. However, the line measured was fairly broad and does not give a sensitive test to the equipment. A more sensitive comparison could only be made with a source/absorber combination which displayed a linewidth much closer to the natural Co^{57} linewidth.

The more conventional leadscrew suspension constructed here gave velocity instabilities very similar in magnitude to those observed for the oil supported suspension. This suspension system is, however, expected to be somewhat better than the latter system, providing that large weights are not to be transported, as the drive system used with it is felt to be inferior. This drive system could be greatly improved by the inclusion of a ball disk integrator, or any other variable speed transmission, with greater torque capabilities and the flywheel used in the drive system for the oil supported suspension.

In both suspension systems tried velocity fluctuations were present as indicated by a frequency change in the output of the velocity monitoring system. As observed on an oscilloscope these frequency changes were greater than a few percent. At the present time it is felt that these fluctuations are too large to enable the performance of the proposed experiment. The leadscrew suspension still provides some hope as an improvement of the drive system may reduce velocity fluctuations to a level at which a serious attempt at such an experiment could be undertaken. It is felt that the velocity stabilities in this case would have to

be less than 1% and preferably close to 0.1%. Such stability is at least an order of magnitude greater than that achieved here.




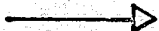

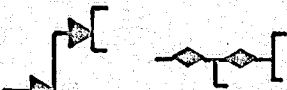
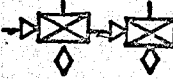


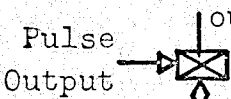




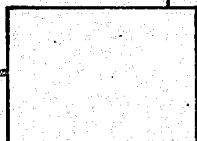
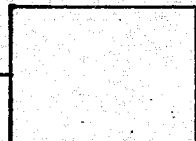
BIBLIOGRAPHY

1. Wells. MSc Thesis, U.B.C., November 1965
2. Woodrow. MSc Thesis, U.B.C., April 1964
3. P. A. Flinn. R.S.I. 34 12 1422
4. R. Booth - C. E. Violet. N.I.M. 25 1963
5. R. H. Nussbaum & F. Gerstenfeld. American Journal of Physics, Jan. 1966
6. R. Zane. N.I.M. 43 1966
7. E. Kankaleit. R.S.I. 35 2 194
8. H. Frauenfelder. 1963. "The Mossbauer Effect" 2nd printing with corrections and additions. Benjamin, 1963
9. E. W. Montroll & R. B. Potts. Phys. Rev 100, 525 (1955)
10. A. A. Maradudin in "Astrophysics and the Many Body Problem: 1962 Brandeis Lectures" Vol. 2. Benjamin 1963
11. A. A. Maradudin & P. A. Flinn. Phys. Rev. 126 2059 (1962)
12. W. C. Overton Jr. & E. Dent. U.S. Naval Research Laboratory Report 5252 Washington 25
13. F. C. Dawber & R. J. Elliot, 1963. Proc. Royal Soc. 273 222 (1963)
14. Roderich Cameron. MSc Thesis, U.B.C., June 1963
15. R. J. Pomeroy, MSc Thesis, U.B.C., July 1963
16. D. M. J. Compton & A. H. Schoen. 1962 ed. "The Mossbauer Effect. Proceedings of the Second International Conference", Wiley 1962
17. A. J. Bearden 1964: ed "Third International Conference on the Mossbauer Effect" Rev. Mod. Phys. 36 737 1964
18. A. J. F. Boyle & H. E. Hall 1962, Rep. Prog. Phys. XXV 441 (1962)
19. R. Brout & Wm. Visscher 1962, Phys. Rev. Let. 9 54 1962

20. S. Margulies & J. R. Ehrman. 1961. N.I.M. 12 131 (1961).
21. J. G. Dash, R. H. Nussbaum. Phys. Rev. Let. 16 144 (1966).
22. R. H. Nussbaum, J. G. Dash. Phys. Stat. Sol. 19 k31 1967
23. R. H. Nussbaum, J. G. Dash. "Mossbauer Emission from Atoms in Relaxing Localized Modes" to be published.
24. L. R. Walker, G. K. Wertheim & V. Jascarino, Interpretation of the Fe⁵⁷ Isomer Shift Phys. Rev. Letters 6, 98, 1961.
25. B. D. Josephson, Temperature Dependent Shift of Gamma Rays Emitted by a Solid. Phy. Rev. Letters 4, 341 (1960).
26. H. Frauenfelder, D. E. Nagle, K. D. Taylor, D. R. F. Cochran & W. M. Vissher, Phys. Rev. 126 (1962) 1065.

APPENDIX A

LIST OF D.E.C. SYMBOLISM

| | | |
|---|---|--|
|  Negative Logic Level |  Positive Logic Level |  Negative Pulse |
|  Positive Pulse |  Nonstandard Signal |  Branch Points |
|  |  |  Common Pulse Lines |
|  Pulse Output output Level Input Diode Capacitor Diode Gate | |  Clamped Load |
|  Base Input Collector Output Emitter |  Diode Inputs Collector Emitter Node Input Diode Gate | |
|  Flip Flop Zero Output One Output (Negative when FF is one Ground when FF is zero) Direct Clear Direct Set Zero Input One Input | | |
|  Input Level Output is Neg. During Delay Delay |  Input Output General Element | |

APPENDIX B

PROGRAM 1

```

      TYPE 9
9  ;FORMAT(/,"MOSS.ONE",/)
8  ;FORMAT(/,"TYPE IN N",/)
      TYPE 8
      ACCEPT 10,N
      DIMENSION A(8),VEL(2),CNT(2),TME(2)
      VEL(1)=.0
      VEL(2)=.0
      CNT(1)=.0
      CNT(2)=.0
      TME(1)=.0
      TME(2)=.0
      DO 1 I=1,N
      DO 2 J=1,8
      ACCEPT 11,A(J)
2  ;CONTINUE
      IJ=I/2
      IF(I-2*IJ)4,3,4
3  ;K=1
      GO TO 5
4  ;K=2
5  ;VEL(K)=VEL(K)+2.227*A(4)/A(3)
      TME(K)=TME(K)+A(3)/7040.0
      CNT(K)=CNT(K)+(A(7)-A(6))
1  ;CONTINUE
      NJ=N/2
      P=NJ
      VEL(1)=VEL(1)/P
      CNTR=CNT(1)/TME(1)
      Q=N-NJ
      VEL(2)=VEL(2)/Q
      CNTNR=CNT(2)/TME(2)
      STATF=SQTF(CNT(1))
      STATR=SQTF(CNT(2))
      TYPE 12,VEL(1),CNTR,CNT(1),STATF
      TYPE 13VEL(2),CNTNR,CNT(2),STATR
10 ;FORMAT(I)
11 ;FORMAT(E)
12 ;FORMAT(/,"VEL.FOR.=",E,"COUNT RATE FOR=",E,"CNT=",E,/, "STATF=",E,/)
13 ;FORMAT(/,"VEL.REV.=",E,"COUNT RATE REV=",E,"CNT=",E,/, "STATR=",E,/)
      STOP
      END

```

\$JOB 79177 J.L. BEVERIDGE

\$IBFTC MAIN

DIMENSION W(6),EJK(6)

DIMENSION LIM(20)

DIMENSION TPRIME(10)

EXTERNAL H, FUNC

REAL NUM

REAL NSIGMA, MUBY2, MUTBY2, LIM

COMMON /BLOC/ Z, Y, MUTBY2, W, EJK, B, EVC

COMMON/BLK/WPR(6), EJKPR(6)

C

C

C

SET CONSTANTS IN THE PROBLEM

DATA NSIGMA, MUBY2, GAMBY2, C, E0, PI/12.58E04, 264.5, 2.25E-09, 3.0E10,

114.4E03, 3.1415926/

READ(5,107) W, WPR, EJK, EJKPR

READ(5,100) M, N, NN

READ(5,101) FPRIME, A, F, T

READ(5,101)(TPRIME(I), I=1, N)

READ(5,106)(LIM(I), I=1, M)

B=GAMBY2*GAMBY2

TAU=F*A*NSIGMA*T

Z=TAU*B/2.0

MUTBY2=MUBY2*T

NUM=EXPFC(MUTBY2)

WRITE(6,103) A, T, F

EE=E0/C

DELV=0.005

DO 6 III=1, N

V=0.0

WRITE(6,104) TPRIME(III), FPRIME

DO 6 J=1, NN

EVC=EE*V

TAUPRM=F*A*NSIGMA*TPRIME(III)

Y=TAUPRM*B

AA=GAMBY2*FPRIME/PI

FF=1.0-FPRIME

AREA1=0.0

YY=0.0

ZZ=LIM(1)

DO 2 I=1, M

AREA1=AREA1+FGAM12(YY, ZZ, H)

```

      YY=ZZ
2     ZZ=LIM(I+1)
      TINF=FF*NUM+2.0*AA*AREA1
      AREA1=0.0
      YY=0.0
      ZZ=LIM(1)
      DO 3 I=1,M
        AREA1=AREA1+FGAU12(YY,ZZ,FUNC)
        YY=ZZ
3     ZZ=LIM(I+1)
      ZZ=0.0
      YY=-LIM(1)
      DO 9 I=1,M
        AREA1=AREA1+FGAU12(YY,ZZ,FUNC)
        ZZ=YY
9     YY=-LIM(I+1)
      TT=FF*NUM+AA*AREA1
      R=TT/TINF
      WRITE(6,105) V,TT,R
      V=V+DELV
6     CONTINUE
7     STOP
100   FORMAT(16I5)
101   FORMAT(8F10.0)
102   FORMAT(1H1)
103   FORMAT(5H1A = ,F12.5,6H T = ,E15.4,9H CM F = ,F7.3)
104   FORMAT(10H0TPRIME = ,E15.4,11H FPRIME = ,E15.4/
11H0,8X,8HVELOCITY,8X,4HT(V),11X,4HR(V)/9X,8H(CM/SEC))
105   FORMAT(1X,F15.3,2F15.6)
106   FORMAT(4E20.5)
107   FORMAT(6F10.0/6F10.0/6F12.5/6F12.5)
      END

```

FORTRAN SOURCE LIST

SOURCE STATEMENT

```

0 # $IBFTC PARLOR
# C SECOND LORENTZIAN CURVE FIT PROGRAM
# C ITERATIVE LEAST SQUARE FIT TO PARABOLA AND UP TO 16 LORENTZIAN
# C ER=RATIO CONVERGENCE CRITERION
# C ERI=RATIO CONVERGENCE CRITERION FOR PEAK I
# C IT=MAXIMUM NUMBER OF ITERATIONS
# C J=IGNORED CHANNELS (IMBEDDED ZEROS MUST BE IGNORED)
# C ABE=SPECTRUM TITLE (UP TO 78 CHARACTERS)
# C P(I,NP)=ESTIMATED LOCATION OF PEAK I
# C H(I,NP)=ESTIMATED HALFWIDTH AT HALF MAXIMUM OF PEAK I
# C Y(I,NP)= COUNTS IN CHANNEL I
# C ZERO TEST DETERMINES BEGIN AND END CHANNELS FOR CALCULATION
# C IF NO PREVIOUS END ZERO, CHANNEL 199 MUST BE ZEROED
# C ZERO TEST DETERMINES END OF EACH DATA SET OF ARBITRARY LENGTH
# C G(I)=AREA, R(I)=AMPLITUDE, OA(I)=OLD AMPLITUDE, P1(I)=CHANGE IN PO
# C NO--DETERMINES WHETHER TO TREAT AS TWO INDEPENDENT 200 CHANNEL
# C SPECTRA OR AS A 400 CHANNEL SPECTRUM
# C KO--DETERMINES WHETHER TO CALCULATE INDEPENDENT LORENTZIAN OR N
# C KCHAN--TELLS WHETHER 200 OR 4000 CHANNELS OF INFORMATION
# C H1(I)=CHANGE IN HALF-WIDTH. S1(I)=CORRECTED HALF WIDTH
# C Y(I) BECOMES COUNTS-PARABOLA, Y2(I)=LORENTZIAN, R1(I)=RESIDUALS,
# C YM=MAXCNTS-PAR, Y2M=MAX LOR., R1M=MAX RES., EM=MAX TOTAL COUNTS
# C G, OA, Y2, R1, YM, Y2M, R1M, EM ARE ALWAYS UNNORMALIZED R, Y CHAN
1 # DIMENSION TA(2)
2 # DIMENSION BASE(20)
3 # DIMENSION P1(20), OA(20), S1(20), H1(20), R(20,2), G(20,2)
4 # DIMENSION IRP(16), IPP(20,2), YIND(6)
5 # DIMENSION A(48,48), B(48), BB(48), AA(16,16,2)
6 # DIMENSION VARS(20,2), VARG(20,2), VARP(20,2), VARB(20,2), VARA(20,2)
7 # DIMENSION VO(2), V1(2), V2(2)
10 # DIMENSION IGNT(2), NLT(2), ARM(2)
11 # DIMENSION H(21,2), P(21,2), ER1(21,2)
12 # DIMENSION PARO(2), PAR1(2), PAR2(2)
13 # DIMENSION Y2(400), R1(400), Y(400), IG(400)
14 # COMMON A,B
15 # DOUBLE PRECISION A,B,C,H,H1,P,P1,BB
16 # INTEGER ABE(13)
17 # DO 1650 KJ=1,3
20 # ASSIGN 1700 TO NN
21 # CALL EOF (5,NN)
22 # READ(5,97) ABE
24 # 97 FORMAT (13A6)
25 # READ(5,51) KCHAN,IT,NO,KO
32 # 51 FORMAT(I3,I2,2I1)
33 # ICHAN=KCHAN/200
34 # IF(NO.NE.0) ICHAN=1
37 # READ(5,52) IPLOT,ER,FL
41 # 52 FORMAT(I1,2F7.3)
42 # IF(IPLOT.NE.2) GO TO 55
45 # READ(5,53) IPLOT1,IPLOT2,IPLOT3,IPLOT4
52 # 53 FORMAT(4I1)
53 # IF(IPLOT4.NE.0) GO TO 55
56 # DO 56 NP=1,ICHAN
57 # READ(5,54) (IPP(I,NP),I=1,20)
64 # 54 FORMAT(20I2)

```

FORTRAN SOURCE LIST PARLOR

SOURCE STATEMENT

```

65 # 56 CONTINUE
67 # 55 CONTINUE
70 # IF(IPL0T.NE.1) GO TO 65
73 # IPL0T1=0
74 # IPL0T2=0
75 # IPL0T3=1
76 # IPL0T4=1
77 # 65 CONTINUE
100 # DO 59 I=1,400
101 # 59 IG(I)=1
103 # DO 91 NP=1,ICHAN
104 # DO 95 NL=1,16
105 # READ (5,94) P(NL,NP),H(NL,NP),ER1(NL,NP)
106 # 94 FORMAT(3F7.0)
107 # IF(ER1(NL,NP).EQ.0.0) ER1(NL,NP)=ER
112 # IF (H(NL,NP).EQ.0.0) GO TO 91
115 # 95 CONTINUE
117 # 91 NLT(NP)=NL-1
121 # AM=1.E6
122 # JAM=0
123 # EM=0.0
124 # Y2M=0.0
125 # YM=0.0
126 # DO 98 I=1,400
127 # READ(5,99) J,YN
131 # 99 FORMAT(I3,F20.0)
132 # IF (J.EQ.0) GO TO 40
135 # IG(J) =0
136 # Y(J)=YN
137 # 98 CONTINUE
141 # 40 CONTINUE
142 # IGN=I-1
143 # IGNT(1) = KCHAN-IGN
144 # DO 101 M=1,400
145 # IF(IG(M).NE.0) GO TO 101
150 # IF(Y(M).GT.EM) EM=Y(M)
153 # 101 CONTINUE
155 # LCHAN=3
156 # KCHAN=KCHAN/ICHAN
157 # DO 1625 NP=1,ICHAN
160 # TA(NP)=0.
161 # ICOUNT=0
162 # RM=0.0
163 # JRM=0
164 # TQ=FLOAT(NP-1)
165 # IGN=IGNT(NP)
166 # NL=NLT(NP)
167 # DO 105 N1=LCHAN,KCHAN
170 # IF(IG(N1).NE.0) GO TO 105
173 # IF(Y(N1).EQ.0.0) IG(N1)=2
176 # IF(Y(N1).NE.0.0) GO TO 106
201 # 105 CONTINUE
203 # 106 DO 107 N=N1,KCHAN
204 # IF(IG(N).NE.0) GO TO 107
207 # IF(Y(N).EQ.0.0) GO TO 109

```


FORTRAN SOURCE LIST PARLOR

SOURCE STATEMENT

```

212 # 107    CONTINUE
214 # 109      N=N-1
215 #      DO 108 L=N,KCHAN
216 # 108    IG(L)=IG(L)+2
220 #      IF(N.EQ.KCHAN) IG(N)=IG(N)-2
223 #      WRITE (6,735) ABE,NP
224 #      IF(NP.EQ.1) LCHAN=1
227 #      WRITE(6,112) IPLOT,ER,IT,(IG(I),I=LCHAN,KCHAN)
234 # 112    FORMAT(7H0IPLOT ,I1/,4H ER ,F7.3/,4H IT ,I4/,4(4H IG ,100I1/))
235 #      WRITE(6,114) (H(NY,NP),NY=1,NL)
242 #      WRITE(6,115) (P(NY,NP),NY=1,NL)
247 #      DO 117 I=1,NL
250 #      IF(ER1( I,NP).EQ.ER) GO TO 117
253 #      WRITE(6,116) (ER1(NY,NP),NY=1,NL)
260 #      GO TO 118
261 # 117    CONTINUE
263 # 118    CONTINUE
264 # 114    FORMAT (1X,3HH ,16F8.3)
265 # 115    FORMAT (1X,3HP ,16F8.3)
266 # 116    FORMAT (1X,3HER1 ,16F8.5,///)
    # C      NORMALIZE COUNTS,DO PRELIMINARY CALCULATIONS
267 #      DO 128 I=N1,N
270 #      IF(IG(I).EQ.3) WRITE(6,111) I
273 # 111    FORMAT(/8H WARNING,5X,7HCHANNEL ,I4, 17H HAS BEEN IGNORED )
274 # 128    Y(I)=Y(I)/EM
    # C      Y = NORMALIZED COUNTS
276 #      L1=3*NL+3
277 #      DO 157 I=1,NL
300 #      H(I,NP)=1.0/(H(I,NP) *H(I,NP))
301 # 157    OA(I)=0.0
303 #      LIM=0
304 #      LIMQ=0
305 #      KING=-1
306 #      GO TO 170
307 # 164    KING=1
310 # 165    DO 167 I=1,NL
311 # 167    OA(I)=R(I,NP)
    # C      FILL LEAST SQUARES MATRIX
313 # 170    DO 200 J=1,L1
314 #      BB(J) = 0.0
315 #      DO 200 I=1,L1
316 #      A(I,J)=0.0
317 # 200    CONTINUE
322 #      DO 300 K=N1,N
323 #      IF(IG( K).NE.0) GO TO 300
326 #      C=K
327 #      DO 250 I=1,NL
330 #      J=3*I
331 #      B(J-2)=1.0/(1.0+H(I,NP)*(C-P(I,NP))**2)
332 #      B(J-1)=B(J-2)*B(J-2)*(C-P(I,NP))
333 # 250    B(J)=B(J-1)*(C-P(I,NP))
335 #      C=C-200.*TQ
336 #      DO 260 I=1,3
337 #      KQT=(L1+I-3)
340 # 260    B(KQT)=C**(I-1)

```

SOURCE STATEMENT

```

342 #      DO 300 J=1,L1
343 #      BB(J) = BB(J) + B(J)*Y(K)
344 #      DO 300 I =1,J
345 #      A(I,J)=A(I,J)+B(I)*B(J)
346 #      300 CONTINUE
352 #      DO 310 I=1,L1
353 #      310 B(I) = BB(I)
# C      SOLVE LEAST SQ. MATRIX
355 #      DO 320 J=1,L1
356 #      DO 320 I=1,J
357 #      320 A(J,I)= A(I,J)
362 #      350 CALL DPVINE(L1,KING,ISIG)
363 #      IF(ISIG.NE.0) GO TO 1600
366 #      ICOUNT=ICOUNT+1
# C      CORRECT PEAK LOCATION AND HALF-WIDTH. IF PEAK OK PRINT RESULTS
367 #      DO 400 IQ=1,NL
370 #      JQ=3*IQ
371 #      R(IQ,NP)=B(JQ-2)
# C      R IS NORMALIZED
372 #      H1(IQ)=-B(JQ)/R(IQ,NP)
373 #      IF ((H(IQ,NP)+H1(IQ)).GT. 0.0) GO TO 400
376 #      374 X2=H(IQ,NP)+H1(IQ)
377 #      LIMQ = LIMQ +1
400 #      IF (LIMQ.GT.10) GO TO 375
403 #      H(IQ,NP)=1.1*H(IQ,NP)
404 #      GO TO 390
405 #      375 IF(LIMQ.GT.20) GO TO 410
410 #      IF(LIMQ.EQ.11) H(IQ,NP)=H(IQ,NP) /((1.1)**10)
413 #      H(IQ,NP)=H(IQ,NP)/1.1
414 #      390 X1=1.0/SQRT(H(IQ,NP))
415 #      WRITE(6,405)IQ,X1,X2
416 #      405 FORMAT(/10X,29HHALF-WIDTH CORRECTED FOR PEAK,I4,4H TO,F7.2,25H
#      1 ATTEMPTED SOLUTION =,F9.3)
417 #      GO TO 165
420 #      400 CONTINUE
422 #      GO TO 430
423 #      410 WRITE(6,412)IQ
424 #      412 FORMAT(/34H WRONG HALFWIDTH ESTIMATE FOR PEAK,I5)
425 #      GO TO 1600
426 #      430 WRITE(6,435)
427 #      435 FORMAT(/9X,4HPeak,5X,12HNEW POSITION,7X,13HNEW HALFWIDTH,9X,10H
#      1W HEIGHT ,10X,8HNEW AREA )
430 #      LIMQ=0
431 #      DO 450 I=1,NL
432 #      J=3*I
433 #      P1(I)=B( J-1)/(2.0*H(I,NP)*R(I,NP))
434 #      P(I,NP)=P(I,NP) + P1(I)
435 #      H(I,NP)=H(I,NP) + 0.9*H1(I)
436 #      S1(I)=1.0/SQRT(H(I,NP))
437 #      R(I,NP)=R(I,NP)*EM
# C      R IS NOW UNNORMALIZED. WILL REMAIN SO UNTIL NEXT ITERATION
440 #      G(I,NP)=S1(I)*R(I,NP)*3.14159
441 #      WRITE(6,455) I,P(I,NP),S1(I),R(I,NP),G(I,NP)
442 #      455 FORMAT(8X,I3,2F20.6,2E20.8)
443 #      450 CONTINUE

```

SOURCE STATEMENT

```

# C      TEST NUMBER OF ITERATIONS AND CONVERGENCE
445 #      LIM = LIM + 1
446 #      IF(LIM.LE.IT)GO TO 457
451 #      WRITE(6,456)
452 # 456  FORMAT(//20X,53HCONVERGENCE NOT MET IN SPECIFIED NUMBER OF ITERA
#      IONS,/)
453 #      GO TO 1600
454 # 457  DO 460 I=1,NL
455 #      IF(ABS(H1(I)/H(I,NP)).GT.ER1(I,NP)) GO TO 165
460 #      IF(ABS(P1(I)/P(I,NP)).GT.ER1(I, NP)) GO TO 165
463 #      IF(ABS((R(I,NP)-OA(I))/R(I,NP)).GT.ER1(I,NP)) GO TO 165
466 # 459  IF(KING.EQ.(-1)) GO TO 164
471 # 460  CONTINUE
# C      PRINT FIT AND DATA FOR EACH CHANNEL. FIND MAXIMA
473 #      WRITE(6,461) ICOUNT
474 # 461  FORMAT(// 12H DPVINE USED ,I4,6H TIMES //)
475 #      PARA0 = B(L1-2)*EM
476 #      PARA1 = B(L1-1)*EM
477 #      PARA2 = B(L1)*EM
500 #      PAR0(NP)=PARA0-TQ*200.*(PARA1-200.*PARA2)
501 #      PAR1(NP)=PARA1-400.*TQ*PARA2
502 #      PAR2(NP)=PARA2
503 #      BM=PARA0-PARA1*PARA1/(4.0*PARA2)
504 #      WRITE (6,735) ABE,NP
505 #      WRITE(6,465)
506 # 465  FORMAT(///,7X,5HCHNL.,11X,6HCOUNTS,12X,8HPARABOLA,8X,15HCOUNTS-P
#      LABOLA,8X,11HLORENTZIANS,10X,8HRESIDUAL )
507 #      S=0.0
510 #      DO 500 K=N1,N
511 #      IF(IG(K).NE.0) GO TO 500
514 #      Y2(K)=0.0
515 #      C=K
516 #      DO 480 I=1,NL
517 # 480  Y2(K)=Y2(K)+R(I,NP)/(1.0+H(I,NP)*(C-P(I,NP))**2)
521 #      PAR= PAR0(NP)+PAR1(NP)*C +PAR2(NP)*C*C
522 #      HOLD=Y(K)*EM
523 #      Y(K)=HOLD-PAR
# C      Y NOW EQUALS UNNORMALIZED COUNTS-PARABOLA
524 #      R1(K)=Y(K)-Y2(K)
525 #      IF(YM.GT.Y(K)) YM=Y(K)
530 #      IF(Y2M.GT.Y2(K)) Y2M=Y2(K)
533 #      IF(RM.LT.ABS(R1(K))) JRM=K
536 #      IF(RM.LT.ABS(R1(K))) RM=ABS(R1(K))
541 #      S=S+R1(K)*R1(K)
542 #      WRITE(6,490) K,HOLD,PAR,Y(K),Y2(K),R1(K)
543 # 490  FORMAT(1X,I10,F18.3,4F20.3)
544 # 500  CONTINUE
546 #      IF(KO.EQ.0) GO TO 506
551 #      WRITE (6,735) ABE,NP
552 #      NZ=6
553 #      IF( (NL.LE.6) .NZ=NL
556 #      WRITE(6,501)
557 # 501  FORMAT (//,39X,24HINDEPENDENT LORENTZIANS ,39X,10HLORENTZIAN ,6X
#      110HCALCULATED ,/,105X,3HSUM,10X,10HLORENTZIAN )
560 #      WRITE(6,502)

```

SOURCE STATEMENT

```

561 # 502 FORMAT(1X,5HCHNL.,6X,3HONE,12X,3HTWO,11X,5HTHREE,11X,4HFOUR,11X,
# 1 4HFIVE,12X,3HSIX,///)
562 # DO 505 K=N1,N
563 # IF(IG(K).NE.0) GO TO 505
566 # YSUM=0.0
567 # DO 507 I=1,6
570 # 507 YIND(I)=0.0
572 # C=K
573 # DO 503 I=1,NZ
574 # YIND(I)=R(I,NP)/(1.0+H(I,NP)*(C-P(I,NP))**2)
575 # YSUM=YIND(I)+YSUM
576 # 503 CONTINUE
600 # WRITE(6,504) K,(YIND(I),I=1,6),YSUM,Y2(K)
605 # 504 FORMAT(1X,I3,2X,6F15.5,2F18.6)
606 # 505 CONTINUE
610 # 506 CONTINUE
611 # SKKK=FLOAT(N-N1-IGN-L1)
612 # D=SQRT(S/SKKK)
613 # WRITE (6,735) ABE,NP
614 # WRITE(6,510)D,EM
615 # 510 FORMAT(///8X,30HAVERAGE MEAN SQUARE RESIDUAL =,E17.8,///8X,26HMAX
# 1UM NUMBER OF COUNTS =,F10.0,/)
616 # WRITE(6,515)PARA0,PARA1,PARA2
617 # 515 FORMAT(8X,11HPARABOLA =(,E15.8,5H) + (,E15.8,10H)*CHNL + (,E15.8
# 111H)*CHNL*CHNL,/)
620 # IF (NP.EQ.1) GO TO 517
623 # WRITE(6,516)
624 # 516 FORMAT(1X,20H CHNL. BEGINS AT 201 )
625 # WRITE(6,515) PAR0(NP),PAR1(NP),PAR2(NP)
626 # 517 CONTINUE
627 # IF(NP.NE.1.AND.AM.GT.RM) WRITE(6,521) AM,JAM
632 # IF(AM.LT.RM) WRITE(6,521) RM,JRM
635 # IF(AM.GT.RM) WRITE(6,520) RM,JRM
640 # 520 FORMAT(8X,18HMAXIMUM RESIDUAL =,E18.8,3X,10HAT CHANNEL,I6)
641 # 521 FORMAT(8X,39HMAXIMUM RESIDUAL FOR TOTAL SPECTRUM IS ,E16.8,3X,
# 1 10HAT CHANNEL ,I5 )
642 # AM=RM
643 # JAM=JRM
644 # ARM(NP)=0.0
645 # DO 525 I=1,NL
646 # 525 ARM(NP)=ARM(NP)+G(I,NP)
650 # WRITE(6,530) ARM(NP)
651 # 530 FORMAT(/8X,12HTOTAL AREA =,E18.8///)
652 # IF(NL.GT.16) GO TO 716
655 # DO 709 I=1,16
656 # 709 IRP(I)=I
660 # WRITE(6,721)(IRP(I),I=1,NL)
665 # 721 FORMAT(//29X,20HAREA FRACTION MATRIX,///1X,4HPEAK,16I7)
666 # DO 725 I=1,NL
667 # AA(I,I,NP) = G(I,NP)/ARM(NP)
670 # I1=I+1
671 # DO725 J=I1,NL
672 # AA(I,J,NP) = G(I,NP)/G(J,NP)
673 # AA(J,I,NP) = G(J,NP)/G(I,NP)
674 # 725 CONTINUE

```

SOURCE STATEMENT

```

677 #      DO 730 I=1,NL
700 #      WRITE(6,720) I,(AA(I,J,NP),J=1,NL)
705 # 730   CONTINUE
      # C   CALCULATE SUBTRACT MATRIX AND PRINT
      # C   SUBTRACT MATRIX-LOWER TRIANGLE=AVERAGE POSITION OF THE TWO PEAKS
      # C   SUBTRACT MATRIX-UPPER TRIANGLE=DISTANCE BETWEEN THE TWO PEAKS
707 #      WRITE (6,713) (IRP(I),I=1,NL)
714 # 713   FORMAT(/30X,16H SUBTRACT MATRIX //1X,5H PEAK , 16I7)
715 #      DO 715 I=1,NL
716 #      DO 715 J=1,I
717 #      AA(J,I,NP) = P(I,NP)-P(J,NP)
720 #      AA(I,J,NP) = (P(I,NP)+P(J,NP))/2.
721 # 715   CONTINUE
724 #      DO 716 I=1,NL
725 #      WRITE(6,720) I,(AA(I,J,NP),J=1,NL)
732 # 716   CONTINUE
734 # 720   FORMAT(/1X,I3,3X,16F7.2)
      # C   PRINT FINAL PARAMETERS. DO ERROR ANALYSIS. PRINT RESULTS
735 #      WRITE (6,735) ABE,NP
736 # 735   FORMAT(1H1,13A6,/,7H NP IS ,I1,/)
737 #      WRITE(6,745)
740 # 745   FORMAT(/24X, 10HFINAL DATA)
741 #      WRITE(6,750)
742 # 750   FORMAT(/,6X,4HPEAK,3X,14HFINAL POSITION,3X,15HFINAL HALFWIDTH,7
      #      112HFINAL HEIGHT,9X,10HFINAL AREA,10X,9HBASE-LINE,5X,20HPERCENT T
      #      2NSMISSION )
743 #      DO 770 I=1,NL
744 #      BASE(I)=PAR0(NP)+PAR1(NP)*P(I,NP)+PAR2(NP)*P(I,NP)*P(I,NP)
745 #      YSUM = -R(I,NP)/BASE(I)*100.
746 #      WRITE(6,760) I,P(I,NP),S1(I),R(I,NP),G(I,NP),BASE(I),YSUM
747 # 760   FORMAT( 5X,I4,F14.3,F17.3,5X,3E20.8,F15.2)
750 #      ER1(I,NP)=S1(I)
751 # 770   CONTINUE
753 #      WRITE(6,772) ARM(NP)
754 # 772   FORMAT(54X,13HTOTAL AREA IS ,E18.8)
755 #      IF(NP.GT.1) WRITE(6,775) PARA0,PARA1,PARA2
760 #      IF(NP.GT.1) WRITE(6,516)
763 #      WRITE(6,775) PAR0(NP),PAR1(NP),PAR2(NP)
764 # 775   FORMAT(/17X,4HA0 =,E18.8,/17X,4HA1 =,E18.8,/17X,4HA2 =,E18.8)
765 #      WRITE(6,780)
766 # 780   FORMAT(/24X,14HERROR ANALYSIS,/,16X,4HPEAK,3X,14HVAR, POSITION
      #      13X,15HVAR, HALFWIDTH,7X,12HVAR, HEIGHT,9X,10HVAR, AREA,7X,15H
      #      2R, BASE-LINE)
767 #      VO(NP)=D*SQRT(A(L1-2,L1-2))
770 #      V1(NP)=D*SQRT(A(L1-1,L1-1))
771 #      V2(NP) = D*SQRT(A(L1,L1))
772 #      DO 825 I=1,NL
773 #      VARA(I,NP)=D*SQRT(A(3*I-2,3*I-2))
774 #      COVA = A(3*I-2,3*I-2)/(B(3*I-2)*B(3*I-2))
775 #      COVE = A(3*I,3*I)/(B(3*I)*B(3*I))
776 #      COVAE = A(3*I-2,3*I)/(B(3*I-2)*B(3*I))
777 #      VARH = (COVA+COVE-2.0*COVAE)*H1(I)*H1(I)
000 #      VARS(I,NP)=D*S1(I)*SQRT(VARH)/(2.0*EM*H(I,NP))
001 #      COVD=A(3*I-1,3*I-1)/(B(3*I-1)*B(3*I-1))
002 #      COVXH= 4.0*H(I,NP)*H(I,NP)*A(3*I-2,3*I-2)-8.0*H(I,NP)*A(3*I-2,3*

```

FORTRAN SOURCE LIST PARLOR

SOURCE STATEMENT

```

003 #      COVXH=(COVXH+4.0*A(3*I,3*I))/(2.0*H(I,NP)*B(3*I-2)-2.0*B(3*I))*
004 #      COVYXH=(2.0*H(I,NP)*A(3*I-2,3*I-1)-2.0*A(3*I-1,3*I))
005 #      COVYXH=COVYXH/(B(3*I-1)*(2.0*B(3*I-2)*H(I,NP)-2.0*B(3*I)))
006 #      VARP(I,NP)=D/EM*SQRT(COVD+COVXH*2.0*COVYXH)*ABS(P1(I))
007 #      VARG(I,NP)=(ABS(VARS(I,NP)/S1(I)) + ABS(VARA(I,NP)/R(I,NP)))
      #      1 *ABS(G(I,NP))
010 #      VARB(I,NP)=V0(NP)+V1(NP)+V2(NP)
011 #      WRITE(6,820) I,VARP(I,NP),VARS(I,NP),VARA(I,NP),VARG(I,NP),
      #      1 VARB(I,NP)
012 # 820    FORMAT(15X,I4,F14.3,F17.3,5X,3E20.8)
013 # 825    CONTINUE
015 #      WRITE(6,830) V0(NP),V1(NP),V2(NP)
016 # 830    FORMAT(/,17X,9HVAR, A0 =,E18.8,/17X,9HVAR, A1 =,E18.8, /17X,9HVA
      #      1 A2 =,E18.8)
017 #      TTC = KCHAN/10
020 #      LCHAN=201
021 #      KCHAN=400
022 #      IF(NP.EQ.1) NY2=N1
025 #      GO TO 1625
026 # 1600  IPLOT=0
027 #      TA(NP)=1.
030 #      WRITE(6,1601)
031 # 1601  FORMAT(1X,17HNO PLOTTER OUTPUT )
032 # 1625  CONTINUE
034 #      IF(KJ.EQ.1) MPLOT=0
037 #      IF(IPLOT.EQ.0) GO TO 701
042 #      IF(MPLOT.EQ.0) TC = 0.0
045 #      IF(MPLOT.EQ.0) CALL PLOTS
050 #      MPLOT=1
051 #      IF( KJ.NE.1) CALL PLOT(TC+6.0,0.0,-3)
054 #      TM=BM
055 #      N1=NY2
056 #      KING = 0
057 #      IF(IPLOT1.NE.0)GO TO 580
062 #      KING = 1
063 #      GM=ABS(Y2M)
064 #      IF(IPLOT2.NE.0) GO TO 560
067 #      IF(ABS(YM).GT.GM)GM=ABS(YM)
072 # 560    CONTINUE
073 #      TC = TTC
074 #      CALL RETP(Y2,IG,N1,N,GM,BM,TC,ABE,KING)
075 #      IF(IPLOT2.EQ.0)GO TO 585
100 #      GO TO 620
101 # 580    IF(IPLOT2.NE.0)GO TO 620
104 #      GM=ABS(YM)
105 # 585    CONTINUE
106 #      KING = KING + 2
107 #      TC = TTC
110 #      CALL RETP(Y,IG,N1,N,GM,BM,TC,ABE,KING)
111 # 620    CONTINUE
112 #      IF(IPLOT3.NE.0) GO TO 650
115 #      KING = 5
116 #      CALL PLOT (TC+6.0,0.0,-3)
117 #      BM=TM
120 #      TC = TTC

```

SOURCE STATEMENT

```

121 #      CALL RETP(R1,IG,N1,N,RN,BM,TC,ABE,KING)
122 # 650      CONTINUE
123 #      IF(IPLOT4.NE.0) GO TO 702
126 #      CALL PLOT (TC+6.0,0.0,-3)
127 #      KING = 4
130 #      BM=TM
131 #      AM=0.0
132 #      DO 655 NP=1,ICHAN
133 #      DO 655 I=1,20
134 #      IF(IPP(I,NP).EQ.0) GO TO 655
137 #      M=IPP(I,NP)
140 #      IF(AM.LT.ABS(R(M,NP))) AM=ABS(R(M,NP))
143 # 655      CONTINUE
146 #      DO 700 NP=1,ICHAN
147 #      DO 660 I=1,20
150 #      IF(IPP(I,NP).EQ.0) GO TO 660
153 #      M=IPP(I,NP)
154 #      S1(M)=ER1(M,NP)
155 #      X1=P(M,NP) - 6.0*S1(M)
156 #      X2=P(M,NP) + 6.0*S1(M)
157 #      K1=X1
160 #      K2=X2 + .999
161 #      IF(K1.LT.1) WRITE(6,656) K1
164 #      IF(K1.LT.1) K1=1
167 #      IF(K2.GT.400) WRITE(6,656) K2
172 # 656      FORMAT(/5H K IS,14//)
173 #      DO 659 J=K1,K2
174 #      IF(IG(J).NE.0) GO TO 659
177 #      X=J
200 #      Y(J) = R(M,NP)/(1.+H(M,NP)*(X-P(M,NP))**2)
201 # 659      CONTINUE
203 #      TC=TTC
204 #      CALL RETP(Y,IG,K1,K2,AM,BM,TC,ABE,KING)
205 # 660      CONTINUE
207 # 700      CONTINUE
211 # 702      CONTINUE
212 # 701      CONTINUE
213 #      DO 1630 NP=1,ICHAN
214 #      IF(IA(NP).NE.0.) GO TO 1630
217 #      WRITE(6,735) ABE,NP
220 #      DO 1628 M=3,400
221 #      IF(IG(M).EQ.3) WRITE(6,111) M
224 # 1628      CONTINUE
226 #      WRITE(6,745)
227 #      WRITE(6,750)
230 #      NL=NLT(NP)
231 #      DO 1629 I=1,NL
232 #      BASE(I)=PAR0(NP)+PAR1(NP)*P(I,NP)+PAR2(NP)*P(I,NP)*P(I,NP)
233 #      YSUM = -R(I,NP)/BASE(I)*100.
234 #      WRITE(6,760) I,P(I,NP),ER1(I,NP),R(I,NP),G(I,NP),BASE(I),YSUM
235 # 1629      CONTINUE
237 #      WRITE(6,772) ARM(NP)
240 #      IF(NP.GT.1) WRITE(6,775) PARA0,PARA1,PARA2
243 #      WRITE(6,775) PAR0(NP),PAR1(NP),PAR2(NP)
244 #      WRITE(6,780)

```

FORTRAN SOURCE LIST PARLOR

SOURCE STATEMENT

```

245 #      DO 1632 I=1,NL
246 #      WRITE(6,820) I,VARP(I,NP),VARS(I,NP),VARA(I,NP),VARG(I,NP),
#          1 VARB(I,NP)
247 # 1632 CONTINUE
251 #      WRITE(6,830) VO(NP),V1(NP),V2(NP)
252 #      IF(NL.GT.16) GO TO 1635
255 #      WRITE (6,713) (IRP(I),I=1,NL)
262 #      DO 1635 L=1,NL
263 #      WRITE(6,720) L,(AA(L,K,NP),K=1,NL)
270 # 1635 CONTINUE
272 # 1630 CONTINUE
274 # 1650 CONTINUE
276 # 1700 CONTINUE
277 #      IF(MPLOT.NE.0) CALL PLOTND
302 #      STOP
303 #      END

```


APPENDIX C

An attempt was made to fit the experimental data obtained with the Armco iron source and enriched iron absorber with a theoretical curve using the computer program written by Woodrow (Appendix B). This program calculates the transmission of the six line spectrum of Fe^{57} which is given by

$$R(V) = \frac{\text{Total transmission at velocity}}{\text{Total transmission at velocity}}$$

$$= 1 - f + \sum_{jk} W_{jk} f \frac{\Gamma}{\pi} \int_{-\infty}^{\infty} \frac{dE}{(E+S)^2 + \Gamma^2/4} \exp\left(-\frac{W_{jk} T \Gamma^2/4}{E^2 + \Gamma^2/4}\right)$$

$$\times \left[1 - \Phi\left(\frac{W_{jk} T \Gamma^2/4}{2[(E+S)^2 + \Gamma^2/4]} + \frac{ut}{2}\right)\right] \left[\exp\left(\frac{W_{jk} T \Gamma^2/4}{2[(E+S)^2 + \Gamma^2/4]} + \frac{ut}{2}\right)^2\right]$$

$$\div \exp\left(\frac{(ut)^2}{2} \left[1 - \Phi\left(\frac{ut}{2}\right)\right]\right)$$

where

$$\Phi(x) = \frac{2}{\sqrt{\pi}} \int_0^x e^{-y^2} dy$$

$$T = f a n v_s t$$

f = probability of absorption without recoil

n = number of atoms per cubic centimeter

a = fractional abundance of Fe^{57}

t = source thickness

W_{jk} = probability of the transition

$$S = (1 + v/c) E_0$$

$$\Gamma = 4.5 \times 10^{-9}$$

$$\sigma_0 = 1.4 \times 10^{-18} \text{ cm}^2$$

These same quantities in the absorber are referred to with the same notation but are distinguished by a prime over the appropriate letter. The above impression has been calculated assuming a gaussian distribution of Co^{57} in the source lattice.

The quantities used for this particular application were

Source:

$$\begin{aligned} x &= 0.00057 \text{ inches} \\ n\sigma_0 &= 12.58 \times 10^4 \text{ cm}^2 \\ E_0 &= 14.4 \text{ kev} \\ \mu/2 &= 264.5 \\ f &= 0.85 \\ a &= 0.0217 \\ W_{jk} &= 1/4, 1/6, 1/12, 1/12, 1/6, 1/4 \end{aligned}$$

Absorber:

The parameters for the absorber are the same as for the source except for the thickness and relative abundance of Fe^{57} . The absorber was thought to have a thickness of 0.8 mg/cm^2 and an enrichment of 85% Fe^{57} . This gives

$$x' = 0.00004 \text{ inches}$$

$$a' = 0.85$$

The theoretical curve for such a source absorber combination is shown in Figure 31. This curve shows no resemblance to the ex-

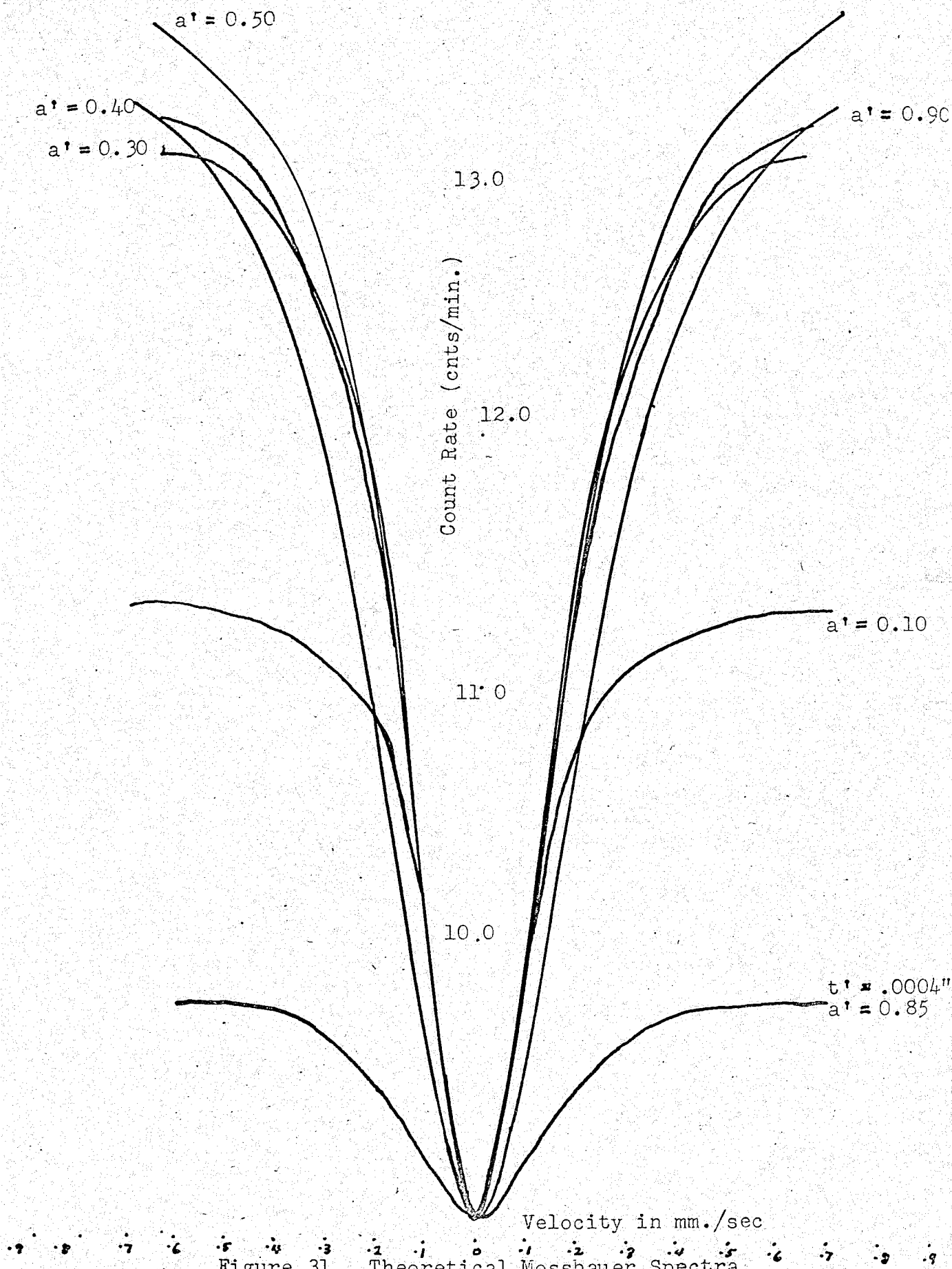
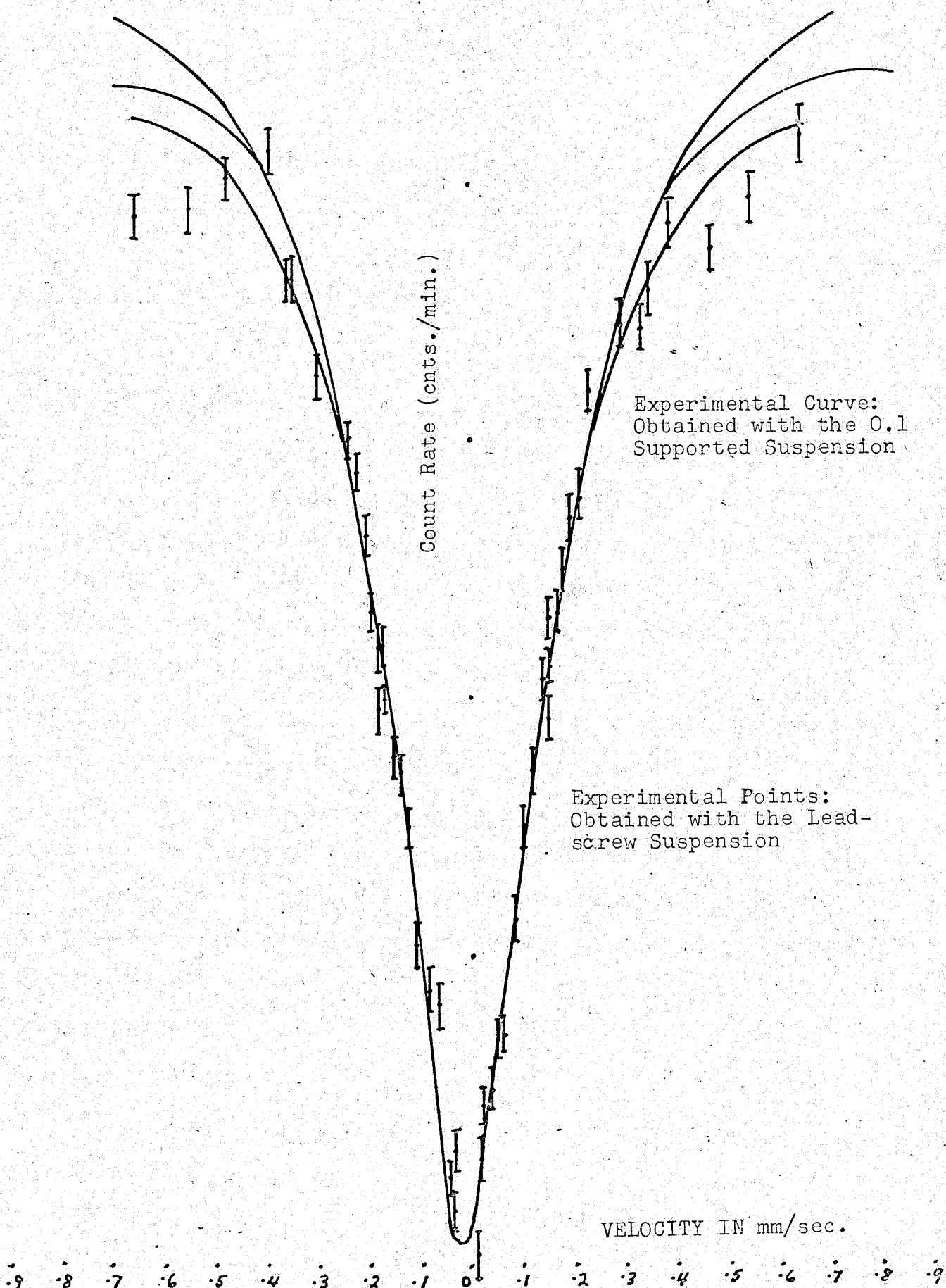


Figure 31. Theoretical Mossbauer Spectra



perimental curve. The other curves in this figure are theoretical curves using an absorber thickness of 0.00035 inches and values of a^1 between 0.10 and 0.90. All these curves are normalized to the experimental data.

Figure 32 shows two theoretical curves with 0.00035 inches and $a^1 = 0.40$ and 0.50 compared to the experimental data. The points plotted here correspond to the data taken with the leadscrew suspension and the solid line the fit to the data taken with the oil suspension. The theoretical curves in the case much more closely approximate the experimental data. The fit obtained for these particular values of t^1 and a^1 does not imply that these are the correct properties of the absorber as there is no reason for assuming uniqueness for these values. However, this does show that the theoretical calculation does produce reasonable results for physically possible absorber parameters. This indicates that the data available for the absorber used was in error and that given correct absorber parameters the experimental line could be compared with the theoretical line as calculated above.